LETTER

doi:10.1038/nature21722

Myt1l safeguards neuronal identity by actively repressing many non-neuronal fates

Moritz Mall[1], Michael S. Kareta[1]†, Soham Chanda[1,2], Henrik Ahlenius[3], Nicholas Perotti[1], Bo Zhou[1,2], Sarah D. Grieder[1], Xuecai Ge[4]†, Sienna Drake[3], Cheen Euong Ang[1], Brandon M. Walker[1], Thomas Vierbuchen[1]†, Daniel R. Fuentes[1], Philip Brennecke[5]†, Kazuhiro R. Nitta[6]†, Arttu Jolma[6], Lars M. Steinmetz[5,7], Jussi Taipale[6,8], Thomas C. Südhof[2] & Marius Wernig[1]

Normal differentiation and induced reprogramming require the activation of target cell programs and silencing of donor cell programs[1,2]. In reprogramming, the same factors are often used to reprogram many different donor cell types[3]. As most developmental repressors, such as RE1-silencing transcription factor (REST) and Groucho (also known as TLE), are considered lineage-specific repressors[4,5], it remains unclear how identical combinations of transcription factors can silence so many different donor programs. Distinct lineage repressors would have to be induced in different donor cell types. Here, by studying the reprogramming of mouse fibroblasts to neurons, we found that the pan neuron-specific transcription factor Myt1-like (Myt1l)[6] exerts its pro-neuronal function by direct repression of many different somatic lineage programs except the neuronal program. The repressive function of Myt1l is mediated via recruitment of a complex containing Sin3b by binding to a previously uncharacterized N-terminal domain. In agreement with its repressive function, the genomic binding sites of Myt1l are similar in neurons and fibroblasts and are preferentially in an open chromatin configuration. The Notch signalling pathway is repressed by Myt1l through silencing of several members, including Hes1. Acute knockdown of Myt1l in the developing mouse brain mimicked a Notch gain-of-function phenotype, suggesting that Myt1l allows newborn neurons to escape Notch activation during normal development. Depletion of Myt1l in primary postmitotic neurons de-repressed non-neuronal programs and impaired neuronal gene expression and function, indicating that many somatic lineage programs are actively and persistently repressed by Myt1l to maintain neuronal identity. It is now tempting to speculate that similar 'many-but-one' lineage repressors exist for other cell fates; such repressors, in combination with lineage-specific activators, would be prime candidates for use in reprogramming additional cell types.

The combination of the three transcription factors Ascl1, Brn2, and Myt1l has been shown to reprogram fibroblasts and other somatic cells into induced neuronal (iN) cells[7]. Ascl1 acts as an 'on-target' pioneer factor to activate the neuronal program, whereas access of Brn2 to the chromatin is context-dependent and facilitates reprogramming later on[8]. Although Ascl1 alone is sufficient to generate iN cells, endogenous Myt1l is induced during reprogramming and exogenous Myt1l greatly improves the efficiency of reprogramming and the functional maturity of the resulting iN cells[9,10]. To investigate the role of Myt1l in reprogramming, we first raised antibodies specific for mouse and human Myt1l (Extended Data Fig. 1). Chromatin immunoprecipitation followed by DNA sequencing (ChIP–seq) of endogenous Myt1l in fetal neurons (embryonic day (E) 13.5) and ectopic Myt1l in mouse embryonic fibroblasts (MEFs) two days after induction identified 3,325 high-confidence Myt1l peaks that overlapped remarkably well between neurons and MEFs (Fig. 1a, Extended Data Fig. 2, Supplementary Table 1). Thus, similar to the pioneer factor Ascl1, Myt1l can access the majority of its cognate DNA binding sites even in a distantly related cell type. However, unlike Ascl1 targets[8], the chromatin at Myt1l

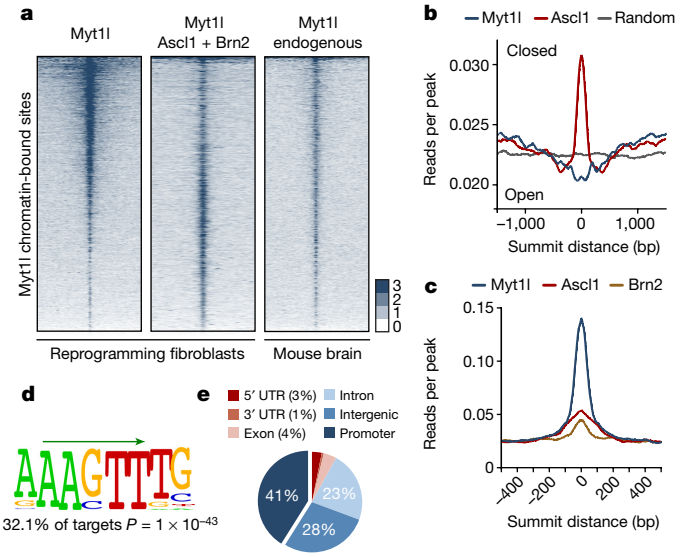

Figure 1 | Context-independent target chromatin access of Myt1l. **a**, Genome-wide occupancy profiles of endogenous Myt1l in E13.5 mouse brains ($n = 2$) or overexpressed Myt1l with ($n = 3$) or without ($n = 2$) *Ascl1* and *Brn2* (also known as *Pou3f2*) in MEFs two days after reprogramming. Corresponding regions are displayed across all datasets ± 2 kb from summits. **b**, Chromatin accessibility based on micrococcal nuclease digestion combined with sequencing (MNase–seq) signal in MEFs[25] shows binding enrichment of Myt1l in open and Ascl1 in closed regions. **c**, Read densities of Ascl1 and Brn2 chromatin binding[8] shows minor overlap at Myt1l-bound regions. **d**, The Myt1l AAGTT core motif (green arrow) is significantly enriched at bound sites across datasets. $P = 1 \times 10^{-43}$, $E = 9.6 \times 10^{-3}$. **e**, Pie chart indicates enrichment of high-confidence Myt1l-bound sites at gene promoters.

[1]Department of Pathology and Institute for Stem Cell Biology and Regenerative Medicine, Stanford University, Stanford, California 94305, USA. [2]Department of Molecular and Cellular Physiology and Howard Hughes Medical Institute, Stanford University, Stanford, California 94305, USA. [3]Department of Clinical Sciences, Division of Neurology and Lund Stem Cell Center, Lund University, 221 84 Lund, Sweden. [4]Department of Developmental Biology, Stanford University, Stanford, California 94305, USA. [5]Department of Genetics, Stanford University, Stanford, California 94305, USA. [6]Division of Functional Genomics and Systems Biology, Department of Medical Biochemistry and Biophysics, Karolinska Institutet, 171 77 Stockholm, Sweden. [7]Genome Biology Unit, European Molecular Biology Laboratory (EMBL), 69117 Heidelberg, Germany. [8]Genome Scale Biology Program, University of Helsinki, 00014 Helsinki, Finland. †Present addresses: Genetics and Genomics Group, Sanford Research, Sioux Falls, SD 57104, USA (M.S.K.); Molecular and Cellular Biology, University of California Merced, Merced, CA 95343, USA (X.G.); Department of Neurobiology, Harvard Medical School, Boston, Massachusetts 02115, USA (T.V.); Leibniz-Institute for Molecular Pharmacology, 13125 Berlin, Germany (P.B.); Division of Genomic Technologies, RIKEN Center for Life Science Technologies, Yokohama 230-0045, Japan (K.R.N.).

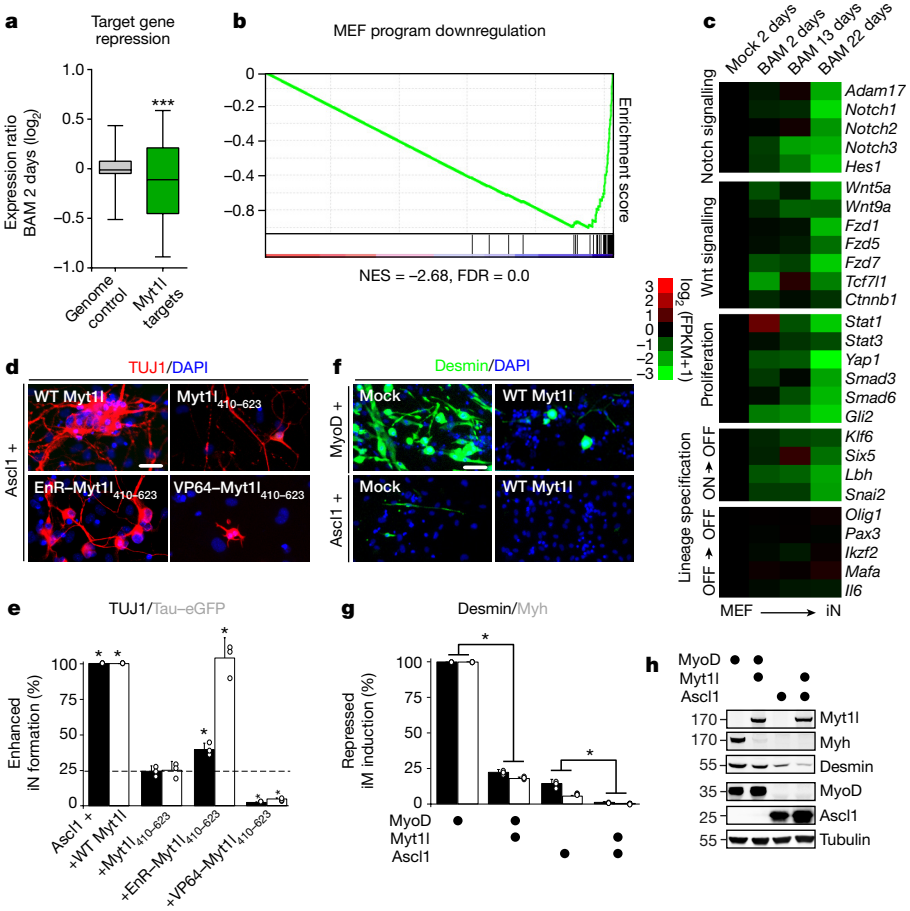

Figure 2 | Myt1l target gene repression dominates induced neurogenesis. a, Repression of promoter-bound (transcription start site (TSS) −5, + 2 kb) Myt1l targets ($n = 1{,}798$) dominates genome-wide expression changes ($n = 33{,}459$) upon two days of reprogramming ($P = 2.78 \times 10^{-12}$, two biological replicates each)[8]. **b**, GSEA identified MEF signature among repressed Myt1l targets. NES, normalized enrichment score; FDR, false discovery rate. **c**, RNA-seq expression values of selected Myt1l targets at indicated time points during reprogramming, normalized to the mock sample; $n = 2$ (ref. 8). Myt1l represses several Notch, Wnt and proliferation factors. Many lineage specifiers are bound and repressed (ON→OFF) or remain repressed (OFF→OFF). FPKM, fragments per kilobase of transcript per million mapped reads. **d**, Immunofluorescence of iN cells derived from MEFs upon reprogramming for 14 days with Ascl1 and wild-type (WT) Myt1l or a non-functional zinc-finger fragment ($Myt1l_{410–623}$) fused to a repressor (EnR) or activator (VP64); TUJ1 (red), DAPI staining (blue). **e**, Conversion efficiency of cells shown in **d** based on TUJ1-positive cells with neuronal morphology (black) or Tau–eGFP expression (white) show partial reprogramming using repressor fusion, with many Tau–eGFP-positive cells without neuronal morphologies. **f**, Immunofluorescence of MEFs upon reprogramming for 14 days with Ascl1 or MyoD without (mock) or with wild-type Myt1l; desmin (green), DAPI staining (blue). **g**, Induced muscle (iM) conversion efficiency of cells shown in **f** based on either desmin (black) or Myh expression (white) shows decreased muscle marker-positive cells upon addition of wild-type Myt1l. **h**, Western blot analysis of cells shown in **f** after 2 days of reprogramming using indicated antibodies (for gel source images see Supplementary Fig. 1). **d**–**g**, Scale bar 50 μm, $n = 3$, error bars show s.d., t-test $^*P < 0.05$.

targets is preferentially open (nucleosome-free) in fibroblasts (Fig. 1b). Hence, Myt1l appears to possess no pioneer factor activity, raising the question why the targets of a neuron-specific transcription factor are easily accessible in fibroblasts. As expected, there was little overlap between the target sites of Myt1l and Ascl1, and the chromatin binding of Myt1l was not strongly affected by Ascl1 and Brn2, indicating that these factors bind and function independent from each other (Fig. 1c, Extended Data Fig. 2d). Conversely, Brn2 targets were co-enriched for both Ascl1 and Myt1l, suggesting that access of Brn2 to chromatin in fibroblasts is strongly directed by other factors[8] (Extended Data Fig. 2d). *De novo* motif discovery identified an AAGTT motif that was significantly enriched in all Myt1l ChIP–seq experiments (Fig. 1d), which is similar to a previously proposed motif[11,12]. Remarkably, almost half of the Myt1l peaks were located in gene promoters, allowing us to associate them with likely target genes (Fig. 1e). Accordingly, we found histone marks associated with active promoters, such as H3K27ac and H3K4me3 enriched at Myt1l-bound regions in MEFs (Extended Data Fig. 2e).

We next assessed the transcriptional effects of Myt1l by RNA sequencing (RNA-seq)[8] (Fig. 2a, Extended Data Fig. 3, Supplementary Table 2). On average, Myt1l targets were significantly downregulated in reprogramming fibroblasts, indicating that Myt1l may be a transcriptional repressor that functions to silence the fibroblast program during reprogramming. Indeed, gene set enrichment analysis (GSEA) showed significant enrichment of MEF signature genes among the repressed Myt1l target genes (Fig. 2b, Supplementary Table 3). To functionally evaluate whether the repressive or activating properties of Myt1l drive iN cell reprogramming, we fused activating (VP64) or repressing (engrailed repressor; EnR) domains to a putative DNA-binding fragment of Myt1l (410–623). The VP64–Myt1l fusion had a strong dominant-negative effect on Ascl1-mediated neuronal conversion, whereas the EnR–Myt1l fusion significantly increased the number of cells expressing the neuron-specific class III β-tubulin TUJ1 and Tau–eGFP compared to the inactive Myt1l fragment (410–623) (Fig. 2d, e). Thus, transcriptional repression is the predominant function of Myt1l during neuronal reprogramming.

We then investigated whether the role of Myt1l might go beyond repressing the fibroblast identity. We found many Myt1l target genes with prominent non-neuronal developmental roles, and most of these

genes were downregulated or remained silent during reprogramming (Fig. 2c). Among the repressed targets were negative regulators of neurogenesis (Notch and Wnt pathway members, as well as *Id3*), key effectors of proliferation (such as Jak/Stat, Hippo, transforming growth factor (TGF) and Shh signalling pathway members), and transcriptional regulators of several non-neuronal lineages. Strikingly, gene ontology analysis of Myt1l-repressed targets showed enrichment of terms associated with several non-neuronal processes (such as cartilage, heart and lung development), suggesting that Myt1l can repress not only the fibroblast program but also additional non-neuronal programs (Extended Data Fig. 3e). The gene expression signatures of MEFs, myocytes, hepatocytes and keratinocytes, but not of neurons, were strongly associated (odds ratio >2) with repressed Myt1l target genes (Extended Data Fig. 3d, Supplementary Table 3). Remarkably, Myt1l motifs were depleted in promoters of neuronal compared to non-neuronal genes, whereas REST motifs were enriched to a similar extent in neuronal versus non-neuronal promoters (Extended Data Fig. 10h). Finally, Myt1l strongly inhibited the formation of myocytes when overexpressed in primary myoblasts during differentiation or together with MyoD in fibroblasts (Fig. 2f–h, Extended Data Fig. 4). The combination of these correlative and functional data suggests that the main physiological function of Myt1l is to repress many non-neuronal programs.

Next, we investigated how Myt1l accomplishes transcriptional repression. To identify critical domains of Myt1l, we tested a collection of systematic Myt1l truncations that in combination with Ascl1 induced neuronal cell reprogramming assay (Fig. 3a, Supplementary Table 4). After ensuring that all Myt1l truncations were stable and localized to the nucleus, we found that a short, 423-amino-acid fragment was sufficient to generate mouse and human iN cells that were molecularly and functionally indistinguishable from those induced by full-length Myt1l (Fig. 3a–d, Extended Data Figs 5, 6). This Myt1l$_{200–623}$ fragment contained a previously uncharacterized N-terminal domain and two zinc-fingers (ZF2 and ZF3), which are presumably responsible for DNA interaction. Surprisingly, the conserved Myt1 domain was dispensable for reprogramming and only one of the three putative DNA-binding zinc-finger domain clusters was required. The presence of three zinc-finger clusters could imply a complex DNA interaction with multiple DNA sites simultaneously bound by different areas of the protein. However, mutating the central zinc-finger cluster to abolish sequence-specific DNA-binding had no effect on Myt1l function[13] (Fig. 3a, b, Extended Data Fig. 7). In a fragment devoid of additional zinc-fingers the same mutations completely abolished Myt1l function, suggesting that the zinc-finger clusters are functionally redundant. *In vitro* DNA binding studies (using systematic evolution of ligands by exponential enrichment (SELEX)) revealed that zinc-finger clusters 2–3 and 4–6 enriched the same AAGTT motif, and ChIP–seq experiments showed that full-length Myt1l and Myt1l$_{200–623}$ bound the same genomic sites during reprogramming (Fig. 3e, Extended Data Fig. 2, Supplementary Tables 1, 5). Thus, multiple DNA-interacting zinc-fingers are not required to engage DNA simultaneously but might simply increase the binding probability of Myt1l to its targets. Notably, downregulated Myt1l targets harbour significantly more AAGTT motifs than do upregulated targets, suggesting that binding affinity affects transcriptional output (Extended Data Fig. 3a).

The N-terminal domain preceding the central zinc-finger cluster was also critical for Myt1l function, because increased truncation of this domain resulted in progressive loss of reprogramming activity (Fig. 3a–d, Extended Data Fig. 5). As Myt1 family members have been reported to interact with Sin3b to mediate gene repression, we tested whether Myt1l can bind this repressive chromatin remodelling complex during neuronal reprogramming[14]. We found that both full-length Myt1l and Myt1l$_{200–623}$, but not Ascl1 or Brn2, could enrich Sin3b by immunoprecipitation (Fig. 3f). Sequence analysis revealed four highly conserved hydrophobic helical peptides within Myt1l$_{200–500}$ that are similar to reported Sin3-interacting domains (SIDs) known to bind the paired amphipathic helix of Sin3b[15] (Extended Data Fig. 8). To identify

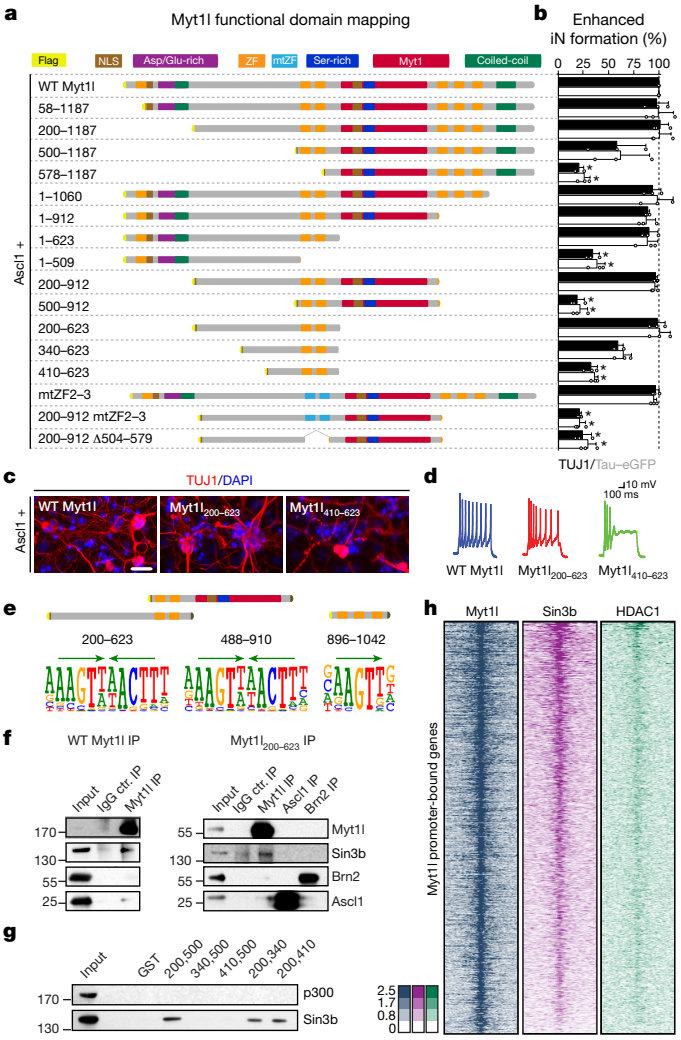

Figure 3 | Characterization of neurogenic and repressive Myt1l domains. a, Truncation and mutation screen identifies Myt1l domains that are essential for induced neurogenesis from MEFs upon reprogramming for 14 days with Ascl1. Highlighted are nuclear localization signals (NLS), aspartic acid/glutamic acid-rich (Asp/Glu-rich), serine-rich (Ser-rich), Myt1 domains, coiled-coil domains, CCHC-type zinc-fingers (ZF) and CCHC-type zinc-finger mutants (mtZF). **b**, Conversion activity compared to wild-type Myt1l based on number of TUJ1-positive cells with neuronal morphology (black) or Tau–eGFP expression (white). $n = 3$, error bars show s.d., *t*-test $^*P < 0.005$. **c**, Representative immunofluorescence of iN cells; TUJ1 (red), DAPI staining (blue), scale bar 50 μm. **d**, Representative action potential (AP) traces of iN cells upon maturation for 21 days on mouse glia. **e**, SELEX DNA-binding experiments with Myt1l zinc-finger fragments enrich the same Myt1l AAGTT core motif (green arrows). **f**, Immunoprecipitation shows binding of endogenous Sin3b to full-length and minimal Myt1l in DNase-treated MEF cell lysates 2 days after transgene overexpression. **g**, GST pull-down from MEF cell lysates identifies minimal Sin3b interaction region within functional Myt1l domain. **h**, Overlapping ChIP–seq chromatin occupancy profiles of overexpressed Myt1l (left), endogenous Sin3b (middle) and HDAC1 (right) at Myt1l promoter target sites in MEFs 2 days after reprogramming induction. $n = 2$, for gel source images see Supplementary Fig. 1.

the SID of Myt1l we performed glutathione *S*-transferase (GST) pull-down experiments and found that the most N-terminal predicted SIDs were necessary and sufficient to bind Sin3b, while no fragment bound the p300 co-activator (Fig. 3g, Extended Data Fig. 8). ChIP–seq experiments showed that 80% of Myt1l targets, including the transcription factor Hes1, were co-bound by the repressive Sin3b–HDAC1 complex

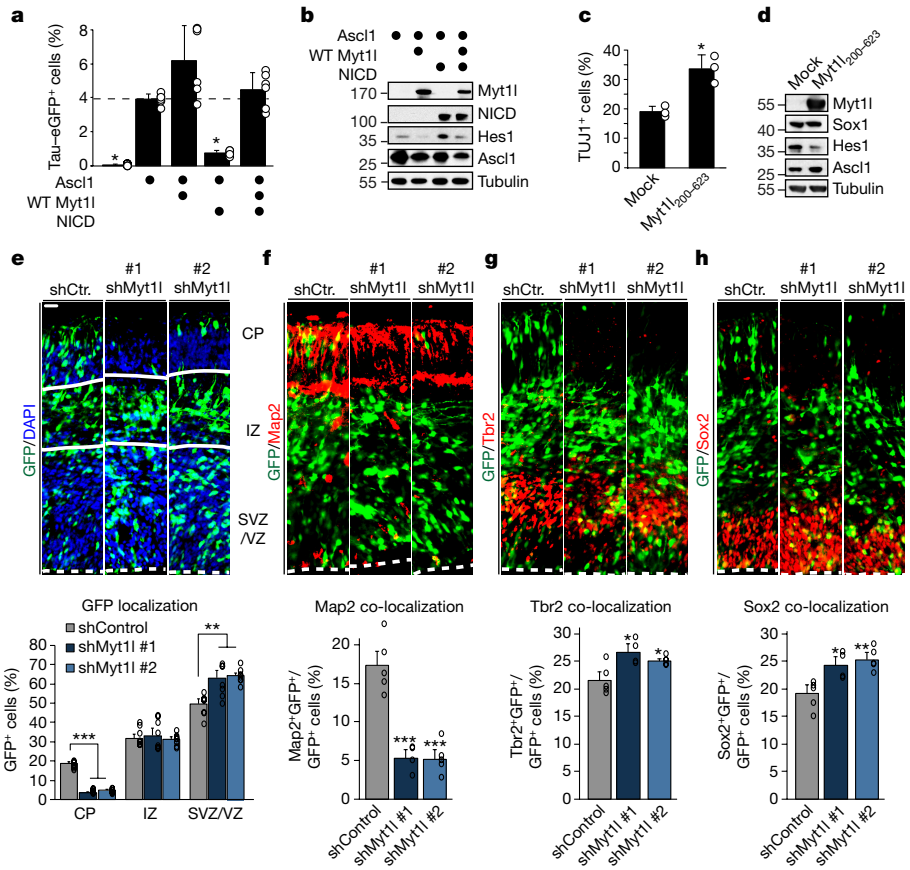

Figure 4 | Myt1l represses Notch and Hes1 activity to promote neurogenesis. a, Fraction of Tau–eGFP$^+$ iN cells derived from MEFs upon reprogramming for 7 days with Ascl1 and wild-type Myt1l, Notch intracellular domain (NICD) or a combination, determined by flow cytometry. $n = 6$, error bars show s.d., *t*-test $^*P < 0.05$. **b**, Western blot analysis of cells shown in **a** using indicated antibodies. **c**, Neuronal differentiation efficiency of mouse NSCs upon overexpression of reverse tetracycline-transactivator (rtTA; mock) or rtTA and Myt1l$_{200–623}$ for 7 days based on TUJ1$^+$ cells with neuronal morphology. $n = 3$, error bars show s.d., *t*-test $^*P < 0.05$. **d**, Western blot analysis of proliferating NSCs upon 7 days of induction of rtTA (mock) alone or with Myt1l$_{200–623}$ using indicated antibodies. **e**, Myt1l knockdown cells exhibit cell positioning defects *in utero*. Control or *Myt1l* shRNA constructs co-expressing GFP were electroporated into E13.5 embryonic mouse brains, and the mice were analysed at E15.5. The percentage of GFP$^+$ cells in each region is shown. CP, cortical plate; IZ, intermediate zone; SVZ/VZ, subventricular zone/ventricular zone ($n = 8$). **f**–**h**, Myt1l knockdown leads to *in vivo* neurogenesis defects. Cortices electroporated in **e** were examined at E15.5 by staining with antibodies against Map2, Tbr2 or Sox2 and the percentage of the GFP$^+$ cells that were also positive for the corresponding markers are shown. $n = 5$ for shControl and shMyt1l #2, $n = 4$ for shMyt1l #1. Scale bar, 25 μm; error bars show s.e.m., *t*-test $^*P < 0.05$, $^{**}P < 0.005$, $^{***}P < 0.0005$. For gel source images see Supplementary Fig. 1.

early during reprogramming (Fig. 3h, Extended Data Fig. 8c). As expected, short hairpin RNA (shRNA)-mediated knockdown of Sin3b abolished iN cell formation, but this could also be due to additional roles of Sin3b[16] (Extended Data Fig. 8e–g).

Like its family member Myt1[17,18], Myt1l targets the Notch signalling pathway on multiple levels (Fig. 2c). Notch signalling inhibits the differentiation of neural progenitor cells through Hes1-mediated repression of proneuronal factors such as Ascl1, but it remains unclear how newborn neurons escape this inhibition[19,20]. We found that Myt1l largely inhibited the negative effect of Notch intracellular domain (NICD) on neuronal reprogramming and reduced the protein levels of Hes1 (Fig. 4a, b, Extended Data Fig. 9a). Chemical inhibition of Notch using *N*-[*N*-(3,5-difluorophenacetyl)-L-alanyl]-*S*-phenylglycine t-butyl ester (DAPT) enhanced Ascl1-mediated Tau–eGFP induction, but did not further enhance reprogramming induced by Ascl1 together with Myt1l (Extended Data Fig. 9b). Combined overexpression of *Ascl1* and *Hes1* in MEFs not only counteracted neuronal reprogramming but also decreased Ascl1 levels without inducing neural stem-cell markers (Extended Data Fig. 9b, c). Surprisingly, *Hes1* overexpression decreased not only Ascl1 protein but also the transgenic *Ascl1* mRNA, suggesting previously unrecognized post-transcriptional regulation of Ascl1 expression (Extended Data Fig. 9d). Addition of Myt1l could not rescue the reprogramming block induced by *Hes1* overexpression, whereas it could rescue the NICD-mediated reprogramming block, demonstrating that Myt1l-mediated Notch inactivation is primarily caused by direct repression of *Hes1* transcription.

To investigate the physiological function of Myt1l during normal neurogenesis, we performed *in utero* electroporation of *Myt1l*-shRNA–GFP constructs into the forebrains of mice at E13.5. Myt1l depletion led to a substantial reduction in the number of electroporated cells in the cortical plate two days later, with a corresponding increase in GFP-positive cells in the ventricular and subventricular zones (Fig. 4e). Moreover, we found a reduced fraction of Map2$^+$ mature neuronal cells among GFP$^+$ cells, and there was a compensatory increase in GFP$^+$ apical (Sox2$^+$) and basal (Tbr2$^+$) progenitors, indicating that acute Myt1l depletion impairs neurogenesis *in vivo* (Fig. 4f–h). Neural stem cells (NSCs) exhibit oscillatory Hes1 expression that triggers anti-phasic expression of proneural factors such as *Ascl1*[19]. To test whether Myt1l could repress *Hes1* and thereby trigger Ascl1 induction and neuronal differentiation, we overexpressed Myt1l$_{200–623}$ in mouse NSCs and observed increased neuronal differentiation (Fig. 4c, Extended Data Fig. 9f). Western blot analysis of NSCs maintained in proliferating conditions with fibroblast growth factor (Fgf) and epidermal growth factor (Egf) showed that overexpression of Myt1l$_{200–623}$ strongly decreased Hes1 and slightly increased Ascl1 protein levels (Fig. 4d). Remarkably, even exogenous Ascl1

protein became stabilized upon Myt1l overexpression in MEFs during reprogramming, further suggesting that Hes1 also blocks Ascl1 post-transcriptionally (Extended Data Fig. 9e). In summary, these findings show that Myt1l can render cells insensitive to Notch signalling and provide a molecular explanation of how newborn neurons can overcome the Notch anti-differentiation stimulus.

Last, we investigated whether Myt1l also represses many non-neuronal programs in primary neurons. RNA-seq of cultured hippocampal neurons showed that shRNA-mediated Myt1l depletion led to de-repression of Myt1l target genes, such as Notch and Wnt pathway members, and overall induced gene ontology terms characteristic of non-neuronal tissues, including cartilage and heart (Extended Data Fig. 10i, j). Fibroblast-, keratinocyte- and hepatocyte-specific gene signatures were more highly enriched among induced than repressed genes (Extended Data Fig. 10g). Importantly, the de-repression of non-neuronal programs was associated with loss of neuronal gene expression and functional properties (Extended Data Fig. 10a–f). Moreover, sequence analysis showed that, in contrast to REST, Myt1l motifs are substantially depleted at neuronal gene promoters, further supporting the 'many-but-neuronal' repressive function of Myt1l (Extended Data Fig. 10h).

In this study, we discovered a new kind of transcriptional repressor. Unlike conventional repressors that inhibit specific lineages, such as REST and Groucho, Myt1l appears to block a multitude of differentiation programs and lineage identities, but not the neuronal lineage. In combination with activating lineage master regulators such as Ascl1, the molecular repressor Myt1l acts in a perfect complementary fashion to enable cell fate determination. Similar pairs of activating and repressing transcription factors may yield optimal reprogramming for other lineages. Finally, our data suggest that the physiological function of Myt1l is to establish and maintain the identity of neurons. Myt1l is the only known transcription factor that is specifically expressed in all neurons throughout life, indicating that active repression of non-neuronal programs is critical for maintaining the neuronal identity[6]. It is possible that the various *Myt1l* mutations recently identified in autism, schizophrenia, major depression, and intellectual disability may affect the neuronal maintenance function of Myt1l rather than neurogenesis[21–24]. If this were the case, it might provide the opportunity to carry out curative interventions even in adult patients.

Online Content Methods, along with any additional Extended Data display items and Source Data, are available in the online version of the paper; references unique to these sections appear only in the online paper.

Received 5 August 2015; accepted 23 February 2017.
Published online 5 April 2017.

1. Schäfer, B. W., Blakely, B. T., Darlington, G. J. & Blau, H. M. Effect of cell history on response to helix-loop-helix family of myogenic regulators. *Nature* **344,** 454–458 (1990).
2. Terranova, R., Pereira, C. F., Du Roure, C., Merkenschlager, M. & Fisher, A. G. Acquisition and extinction of gene expression programs are separable events in heterokaryon reprogramming. *J. Cell Sci.* **119,** 2065–2072 (2006).
3. Xu, J., Du, Y. & Deng, H. Direct lineage reprogramming: strategies, mechanisms, and applications. *Cell Stem Cell* **16,** 119–134 (2015).
4. Santisteban, P., Recacha, P., Metzger, D. E. & Zaret, K. S. Dynamic expression of Groucho-related genes Grg1 and Grg3 in foregut endoderm and antagonism of differentiation. *Dev. Dyn.* **239,** 980–986 (2010).
5. Schoenherr, C. J. & Anderson, D. J. The neuron-restrictive silencer factor (NRSF): a coordinate repressor of multiple neuron-specific genes. *Science* **267,** 1360–1363 (1995).
6. Matsushita, F., Kameyama, T., Kadokawa, Y. & Marunouchi, T. Spatiotemporal expression pattern of Myt/NZF family zinc finger transcription factors during mouse nervous system development. *Dev. Dyn.* **243,** 588–600 (2014).
7. Masserdotti, G., Gascón, S. & Götz, M. Direct neuronal reprogramming: learning from and for development. *Development* **143,** 2494–2510 (2016).
8. Wapinski, O. L. *et al.* Hierarchical mechanisms for direct reprogramming of fibroblasts to neurons. *Cell* **155,** 621–635 (2013).
9. Vierbuchen, T. *et al.* Direct conversion of fibroblasts to functional neurons by defined factors. *Nature* **463,** 1035–1041 (2010).
10. Chanda, S. *et al.* Generation of induced neuronal cells by the single reprogramming factor ASCL1. *Stem Cell Rep.* **3,** 282–296 (2014).
11. Jiang, Y. *et al.* A novel family of Cys-Cys, His-Cys zinc finger transcription factors expressed in developing nervous system and pituitary gland. *J. Biol. Chem.* **271,** 10723–10730 (1996).
12. Yee, K. S. & Yu, V. C. Isolation and characterization of a novel member of the neural zinc finger factor/myelin transcription factor family with transcriptional repression activity. *J. Biol. Chem.* **273,** 5366–5374 (1998).
13. Besold, A. N., Oluyadi, A. A. & Michel, S. L. J. Switching metal ion coordination and DNA recognition in a tandem CCHHC-type zinc finger peptide. *Inorg. Chem.* **52,** 4721–4728 (2013).
14. Romm, E., Nielsen, J. A., Kim, J. G. & Hudson, L. D. Myt1 family recruits histone deacetylase to regulate neural transcription. *J. Neurochem.* **93,** 1444–1453 (2005).
15. Spronk, C. A. *et al.* The Mad1–Sin3B interaction involves a novel helical fold. *Nat. Struct. Biol.* **7,** 1100–1104 (2000).
16. Grzenda, A., Lomberk, G., Zhang, J.-S. & Urrutia, R. Sin3: master scaffold and transcriptional corepressor. *Biochim. Biophys. Acta* **1789,** 443–450 (2009).
17. Vasconcelos, F. F. *et al.* MyT1 counteracts the neural progenitor program to promote vertebrate neurogenesis. *Cell Rep.* **17,** 469–483 (2016).
18. Bellefroid, E. J. *et al.* X-MyT1, a *Xenopus* C2HC-type zinc finger protein with a regulatory function in neuronal differentiation. *Cell* **87,** 1191–1202 (1996).
19. Kageyama, R., Ohtsuka, T., Shimojo, H. & Imayoshi, I. Dynamic Notch signaling in neural progenitor cells and a revised view of lateral inhibition. *Nat. Neurosci.* **11,** 1247–1251 (2008).
20. Axelrod, J. D. Delivering the lateral inhibition punchline: it's all about the timing. *Sci. Signal.* **3,** pe38 (2010).
21. De Rocker, N. *et al.* Refinement of the critical 2p25.3 deletion region: the role of MYT1L in intellectual disability and obesity. *Genet. Med.* **17,** 460–466 (2015).
22. De Rubeis, S. *et al.* Synaptic, transcriptional and chromatin genes disrupted in autism. *Nature* **515,** 209–215 (2014).
23. Lee, Y. *et al.* Microduplications disrupting the *MYT1L* gene (2p25.3) are associated with schizophrenia. *Psychiatr. Genet.* **22,** 206–209 (2012).
24. Li, W. *et al.* Association study of myelin transcription factor 1-like polymorphisms with schizophrenia in Han Chinese population. *Genes Brain Behav.* **11,** 87–93 (2012).
25. Teif, V. B. *et al.* Genome-wide nucleosome positioning during embryonic stem cell development. *Nat. Struct. Mol. Biol.* **19,** 1185–1192 (2012)

Supplementary Information is available in the online version of the paper.

Acknowledgements We acknowledge N. E. Davey for SID motif discovery, U. Litzenburger for initial *in utero* experiments and S. Marro and N. Yucel for primary cell preparations. We thank J. E. Johnson, T. Sudo, R. Kageyama, and T. Stearns for antibodies; G. Mantalas, B. Passarelli, M. Miranda and M. Nguyen for sequencing; and A. Stark and Wernig laboratory members for ideas and discussions. Support was provided by the German Research Foundation to M.M., an NCI training grant (#T32 CA09151), the DHHS and the Spectrum Child Health Research Institute to M.S.K, the Swedish Research Council and Swedish Government Initiative for Strategic Research Areas (StemTherapy) to H.A., the National Institutes of Health to L.M.S., T.C.S. and M.W. and the California Institute for Regenerative Medicine to M.W. T.C.S. is a Howard Hughes Medical Institute Investigator. M.W. is a New York Stem Cell Foundation-Robertson Investigator, a Tashia and John Morgridge Faculty Scholar at the Child Health Research Institute at Stanford, and a Howard Hughes Medical Institute Faculty Scholar.

Author Contributions M.M. was responsible for research design, execution, data analysis, and manuscript preparation. M.S.K. performed and designed the bioinformatics analysis and aided in manuscript preparation. S.C. and B.Z. performed the electrophysiological analysis. H.A. performed the NSC experiments and advised on research design and manuscript preparation. X.G., C.E.A. and S.D. performed *in utero* electroporation. N.P. aided in the biochemical interaction studies. S.D.G. performed the FACS analysis. T.V., B.M.W. and D.R.F. generated constructs. P.B. and L.M.S. performed the sequencing. K.R.N., A.J. and J.T. performed the SELEX. T.C.S. supported the research. M.W. was responsible for supervision and design of research, data interpretation, and manuscript preparation.

Author Information Reprints and permissions information is available at www.nature.com/reprints. The authors declare no competing financial interests. Readers are welcome to comment on the online version of the paper. Publisher's note: Springer Nature remains neutral with regard to jurisdictional claims in published maps and institutional affiliations. Correspondence and requests for materials should be addressed to M.W. (wernig@stanford.edu).

Reviewer Information *Nature* thanks T. Graf and the other anonymous reviewer(s) for their contribution to the peer review of this work.

METHODS

No statistical methods were used to predetermine sample size and the investigators were not blinded to allocation during experiments and outcome assessment.

Reprogramming and efficiency calculation. Third-passage wild-type, heterozygous Tau–eGFP knock-in MEFs or human embryonic fibroblasts were infected with indicated lentivirus (available from us through Addgene or specified in Supplementary Table 4) in MEF medium containing 8 μg/ml polybrene (Sigma) for 16–20 h. Cells were switched into fresh MEF medium containing 2 μg/ml doxycycline (Sigma) to induce transgene expression for 2 days. On day 3 cells were switched into N3 medium (DMEM/F12) containing N2 supplement, B27, 20 μg/ml insulin, penicillin/streptomycin (all from Invitrogen) and doxycycline to continue reprogramming. The medium was changed every 2–3 days for the duration of the reprogramming. To calculate the efficiency of neuronal induction, the total number of Tau–eGFP- and/or TUJ1-expressing cells with complex neurite outgrowth (cells having a spherical cell body and at least one thin process three times the size of their cell body) was counted manually 7 or 14 days after transgene induction by immunofluorescence microscopy. To calculate the efficiency of myocyte-like cell induction, the total number of desmin- and Myh-expressing cells was counted manually 14 days after transgene induction by immunofluorescence microscopy. The quantification was based on the average number of neuronal or myocyte-like cells present in a minimum of 30 randomly selected 20× fields of view from at least three biological replicates. The number of reprogrammed cells was then normalized either to the number of reprogrammed cells in the control condition or to the total number of cells determined by DAPI staining. Tau–eGFP-expressing cells in Fig. 4a and Extended Data Fig. 9b were quantified using a LSRFortessa fluorescence-activated cell analyser (BD Biosciences), on the basis of the average number of TauEGFP-positive cells detected in 60,000–120,000 analysed cells from at least three to six biological replicates.

***In utero* electroporation.** All animal protocols have been IRB approved by Stanford University. For *in utero* electroporation, pregnant CD-1 mice (Charles River) were deeply anaesthetized with isoflurane (Henry Schein), after which the uterine horns were carefully exposed through a midline abdominal incision. pSico constructs encoding both GFP and indicated shRNA-oligos from the same DNA plasmid (1–2 μl of 2 μg/μl) were diluted in PBS containing 0.01% fast green (Sigma) as a tracer and injected *in utero* into the lateral ventricle of mouse embryos at E13.5 using a micropipette made from G-1 glass capillaries (Narishige). After injection, the embryo in the uterus was placed in a 5-mm platinum tweezertrode and five 50-ms square pulses of 25 V with 950-ms intervals were applied with an ECM 830 electroporation system (both from Harvard Apparatus). We performed randomized electroporations of control or Myt1l-targeting shRNAs in the right and left uterine horns of several pregnant mice to avoid any technical effect on the experimental outcome. Then, uterine horns were placed back into the abdominal cavity, and the abdominal wall of the pregnant mouse was sutured. Embryonic brains were harvested and dissected 2 days (E15.5) after electroporation for subsequent immunofluorescence processing and analysis. Brain sections were then co-stained with the indicated antibodies and anti-GFP to identify electroporated cells expressing the indicated knockdown constructs. The distribution of GFP-positive cells in each layer and the fraction of GFP and marker double-positive cells were determined by dividing the number of GFP-positive cells in each layer or the total number of double-positive cells by the total number of GFP-positive cells in the entire section, respectively.

Electrophysiology. Electrophysiological recordings were performed from mouse primary hippocampal neurons 14 days after *in vitro* culture and 11 days after shRNA infection or on MEF-derived induced neuronal (MEF-iN) cells 21 days after transgene induction and 14 days after co-culturing on glia, following previous protocols[9]. In brief, action potentials were recorded using a current-clamp configuration with pipette solution containing (in mM): 130 $KMeSO_3$, 10 NaCl, 2 $MgCl_2$, EGTA 0.5 (for MEF-iN), 1 (for primary cultures), $CaCl_2$ 0.16 (for MEF-iN), 0.1 (for primary cultures), 4 Na_2ATP, 0.4 NaGTP, 14 Tris-creatine phosphate, and 10 HEPES-KOH (pH adjusted to 7.3, 310 mOsm). The bath solution contained (in mM): 140 NaCl, 5 KCl, $CaCl_2$ 2 (for MEF-iN), 3 (for primary cultures), 1 $MgCl_2$, 10 glucose, and 10 HEPES-NaOH (pH 7.4). Membrane potentials were kept around −60 mV using small holding currents, and step currents were injected to elicit action potentials. Recordings of the intrinsic and active membrane properties were performed in the presence of 50 μM picrotoxin, 10 μM CNQX and 50 μM D-AP5 in the bath solution (all from Tocris). The synaptic current recordings were performed in voltage-clamp mode with internal solution containing (in mM): 135 $CsCl_2$, 1 EGTA, 4 Na_2ATP, 1 Na-GTP, 1 QX-314, and 10 HEPES-NaOH (pH adjusted to 7.4, 310 mOsm). α-Amino-3-hydroxy-5-methyl-4-isoxazolepropionic acid (AMPA)-receptor excitatory postsynaptic currents (EPSCs) were pharmacologically isolated by application of 50 μM picrotoxin, and were subsequently blocked by addition of 50 μM CNQX. Evoked synaptic responses were triggered by 1-ms, 1-mA current injection through a local extracellular electrode (FHC concentric bipolar electrode) with a Model 2100 Isolated Pulse Stimulator (A-M Systems). All recordings were performed in whole-cell configuration using a Multiclamp 700B amplifier (Molecular Devices). All average data were analysed from three or more biological replicates using Clampfit 10.4 (Axon Instruments).

Cell line generation and maintenance. MEFs were isolated from wild-type or heterozygous Tau–eGFP knock-in mouse embryos at E13.5 (Jackson Laboratories) after removal of all neural cell-containing tissues. Mouse glial cells were isolated from forebrains of wild-type mice (Jackson Laboratories) at postnatal day 2. Both cell types were maintained in MEF medium (DMEM; Invitrogen) containing 10% cosmic calf serum (CCS; Hyclone), beta-mercaptoethanol (Sigma), non-essential amino acids, sodium pyruvate and penicillin/streptomycin (all from Invitrogen) and passaged three times before experiments. Mouse NSCs were isolated from forebrains at E13.5 or cortex at E14.5 of wild-type mouse embryos. The cells were maintained on PO-laminin-coated tissue culture dishes or as neurospheres in proliferation medium (DMEM/F12) containing N2 or B27 supplement, penicillin/streptomycin (all from Invitrogen), and 20 ng/ml Egf, 10 ng/ml Fgf (both from Peprotech). Cells were infected and kept in proliferation medium for 7 days after transgene induction using doxycycline or changed 1 day after infection to N3 medium (DMEM/F12) containing N2 supplement, B27, 20 μg/ml insulin, penicillin/streptomycin (all from Invitrogen), 1% fetal bovine serum (FBS; Hyclone), and doxycycline to induce differentiation for 7 days. For primary neuronal cultures, the hippocampus of P0 wild-type mouse pups was isolated and cultured on Matrigel-coated plates (Corning) in MEM supplemented with B27, glucose, transferrin and 5% FBS. Two days after plating, the medium was supplemented with 2 mM Ara-C (Sigma) as described previously[26]. Primary myoblasts were isolated and cultured on collagen-coated plates (Corning) in DMEM supplemented with 20% FBS and penicillin/streptomycin (Invitrogen) as described[27]. One day after infection and transgene induction using doxycycline, primary myoblasts were transferred into DMEM containing penicillin/streptomycin and 5% horse serum (all from Invitrogen) to induce muscle differentiation for 4 days. The medium for all cells was changed every 2–3 days for the duration of the experiment and all cells were grown at 37 °C and 5% CO_2. Cells tested negative for mycoplasma contamination.

Virus production and infection. Lentiviruses were produced by transfection of lentiviral backbones containing the indicated transgenes together with third-generation packaging plasmids into HEK293 cells following the Trono laboratory protocol[28]. Viruses were concentrated from culture supernatant by ultra-centrifugation (23,000 rpm, 2 h, 4 °C) and cells were infected with three different viral titres. Infected cell populations that were used for reprogramming and genomic analysis were verified by immunofluorescence to contain approximately 70–90% transgene-positive cells 2 days after induction by immunofluorescence microscopy.

Plasmid constructs. DNA constructs were generated by PCR amplification with Phusion polymerase followed by restriction digest using the indicated enzymes and ligation with T4 DNA ligase (all from NEB). Site-directed mutations of Myt1l zinc-fingers 2–3 were generated using the QuikChange Multi Site-Directed Mutagenesis Kit (Agilent Technologies) following the manufacturer's instructions. A complete list of all constructs and primers generated in this study can be found in Supplementary Tables 4 and 6.

Protein expression and purification. Proteins for immunization and GST pull downs were expressed in *E. coli* Rosetta DE3 (Novagen). All His- and His-GST-tagged Myt1l fragments were purified under native conditions using Ni-NTA Agarose (Qiagen) and eluted in bacterial lysis buffer containing (in mM): 20 Tris pH 7.5, 500 NaCl, 1 $MgCl_2$ supplemented with 400 imidazole (all from Sigma). Eluted proteins were dialysed overnight against phosphate buffered saline (PBS) and supplemented with 10% glycerol (both from Sigma) before use or storage at −80 °C.

Antibodies. Polyclonal antibodies against Myt1l were raised in rabbits using recombinant His-tagged mouse mmMyt1l amino acids 171–420. Immune sera were affinity purified against the antigen immobilized on Affigel (Bio-rad) and eluted in buffer containing (in mM): 100 glycine pH 2.7, 150 NaCl followed by 100 glycine pH 2.2, 150 NaCl. 50 ml anti-Ascl1 hybridoma supernatant, 2.5 mg affinity purified anti-Myt1l antibody, and mouse or rabbit control IgG (Sigma) were each coupled to 250 μl protein A sepharose (GE Healthcare) using buffer containing (in mM): 20 dimethyl pimelimidate in 200 $Na_2B_4O_7$ pH 9, blocked with 1,000 Tris pH 8, followed by 200 ethanolamine pH 8, washed with 200 $Na_2B_4O_7$ pH 9, washed with 200 glycine pH 2.2, 150 NaCl, and finally washed extensively using PBS (all from Sigma). A complete list of all primary antibodies used in this study can be found in Supplementary Table 7. Secondary Alexa-conjugated antibodies were used at 1:2,000 (all from Invitrogen), secondary HRP-conjugated antibodies were used at 1:5,000 (all from Jackson Immunoresearch) and secondary IRDye-conjugated antibodies were used at 1:5,000 (all from LI-COR).

Immunofluorescence. Cultured cells were washed with PBS and fixed using 4% paraformaldehyde (PFA; Affymetrix) for 10 min. Cells were then permeabilized in 0.5% Triton X-100 (Sigma) in PBS for 5 min, blocked in a solution of PBS containing 2% bovine serum albumin (BSA; Sigma) for 1 h, and incubated with primary antibody for 1 h at room temperature or overnight at 4 °C. Cells were washed three times for 15 min using blocking solution before being incubated for 30 min with secondary antibodies. For DNA staining, 100 ng/ml DAPI was added to the last washing step (Invitrogen). Embryonic mouse brains were dissected and immersion fixed in 4% PFA overnight; adult mice were transcardially perfused first with PBS followed by ice-cold 4% PFA, then the brains were isolated and post-fixed in 4% PFA overnight. After fixation, embryonic and adult brains were cryoprotected overnight in 30% sucrose in PBS. Embryonic brains were embedded in OCT compound (Sakura), frozen in dry ice, sectioned on a cryostat at 20 μm and mounted on glass slides. Adult brains were sectioned at 40 μm using a freezing sliding microtome. For immunofluorescence, mounted (embryonic) or free-floating (adult) sections were washed in potassium phosphate buffer (KPBS). They were then incubated in KPBS with 0.25% Triton-X100 and 5% normal donkey and goat serum (pre-incubation solution; both from Jackson Immunoresearch) for 1 h at room temperature and incubated with primary antibody in pre-incubation solution overnight at 4 °C. Following washes in KPBS with 0.25% Triton-X100, sections were incubated with secondary antibodies and Hoechst (Invitrogen) in pre-incubation solution for 2 h at room temperature. After final washes in KPBS, free-floating sections were mounted on gelatin-coated slides and sealed using glycerol-based mounting medium. Microscopy images were obtained using a DM6000 B microscope equipped with a 20 × HCX PL air objective (NA 0.4) and a DFC365 FX digital camera (all from Leica).

Immunoprecipitation experiments. For each immunoprecipitation, 20×10^6 MEF cells infected with the indicated transgenes 2 days after induction were lysed in 1 ml cell lysis buffer containing (in mM): 0.5% Tween-20, 50 Tris pH 7.5, 2 EDTA, 1 DTT, 1 PMSF, 5 NaF (all from Sigma), and complete protease inhibitor (Roche) for 15 min at 4 °C. Nuclei were pelleted by centrifugation (3,200 rpm, 1 min, 4 °C) and resuspended in 1 ml NP-40 lysis buffer containing (in mM): 0.5% NP-40, 50 Tris pH 8, 150 NaCl, 2 EDTA, 1 DTT, 1 PMSF, 5 NaF, 5 μg/ml cytochalasin B (all from Sigma), complete protease inhibitor (Roche), and benzonase (Merck). Debris was removed by centrifugation (14,000 rpm, 10 min, 4 °C) and nuclear lysate was pre-cleared by incubation with 15 μl uncoupled protein A beads before addition of 15 μl antibody-coupled beads for 2 h at 4 °C. After binding, the beads were washed extensively in NP-40 lysis buffer and bound proteins were eluted with SDS–PAGE sample buffer.

GST pull-down experiments. For each pull-down, 20×10^6 MEF cells were lysed in 1 ml cell lysis buffer containing (in mM): 0.5% Tween-20, 50 Tris pH 7.5, 2 EDTA, 1 DTT, 1 PMSF, 5 NaF (all from Sigma), and complete protease inhibitor (Roche) for 15 min at 4 °C. Nuclei were pelleted by centrifugation (3,200 rpm, 1 min, 4 °C) and resuspended in 0.5 ml cell lysis buffer containing 500 mM NaCl, 5 μg/ml cytochalasin B (Sigma), and benzonase (Merk). Debris was removed by centrifugation (14,000 rpm, 10 min, 4 °C) and nuclear lysate was diluted with cell lysis buffer 1:1.25 (200 mM NaCl c.f.). 50 μg of GST alone or GST-tagged Myt1l fragments were incubated with 20 μl glutathione sepharose 4B beads (GE Healthcare) in PBS supplemented with 2 μg/ml BSA (Sigma) and complete protease inhibitor (Roche) for 1 h at 4 °C. Beads were then washed extensively in cell lysis buffer containing 200 mM NaCl before addition of diluted nuclear lysate and incubation for 2 h at 4 °C. After binding the beads were washed extensively in cell lysis buffer containing 200 mM NaCl, and bound proteins were eluted with SDS–PAGE sample buffer.

ChIP-seq and computational analysis. For each ChIP-seq experiment, either four brains from wild-type E13.5 mouse embryos or $20–40 \times 10^6$ primary cells 2 days after transgene induction were cross-linked using 1% formaldehyde (EMS) for 10 min followed by lysis in 1 ml swelling buffer containing (in mM): 0.5% NP-40, 5 HEPES pH 7.9, 85 KCl, 1 DTT, 1 PMSF (all from Sigma), and complete protease inhibitors (Roche) for 20 min on ice. Nuclei were pelleted by centrifugation (3,200 rpm, 1 min, 4 °C) and lysed in 1 ml lysis buffer containing (in mM): 1% SDS, 50 Tris pH 8, 10 EDTA, 1 DTT, 1 PMSF (all from Sigma), and complete protease inhibitors (Roche) for 10 min on ice. Chromatin was sheared using a Bioruptor sonicator (Diagenode) until DNA was fragmented to 200–500 bp followed by 1:4 dilution with buffer containing (in mM): 1% Triton X-100, 20 Tris pH 8, 2 EDTA, 150 NaCl, 1 PMSF (all from Sigma), and complete protease inhibitors (Roche). Diluted lysate was pre-cleared by incubation with 15 μl Staph A cells or 50 μl protein A beads before addition of antibody (20 μg Sin3b or 50 μg HDAC1) or 50 μl antibody-coupled beads (Myt1l) overnight at 4 °C. After binding, the antibody-coupled beads were washed extensively in wash buffer containing (in mM): 1% NP-40, 0.05% SDS, 20 Tris pH 8, 250 NaCl, 2 EDTA (all from Sigma), and complete protease inhibitors (Roche). The reactions with uncoupled antibody were supplemented with 15 μl Staph A cells washed extensively in the following three wash buffers containing (in mM): 1% Triton X-100, 0.1% SDS, 20 Tris pH 8, 150 NaCl, 2 EDTA; 1% Triton X-100, 0.1% SDS, 20 Tris pH 8, 500 NaCl, 2 EDTA; and 1% NP-40, 1% DOC, 10 Tris pH 8, 250 LiCl, 1 EDTA. After washing, the bound fraction was eluted in 100 μl elution buffer containing (in mM): 1% SDS, 50 Tris pH 8, 10 EDTA, 100 PMSF and reversed cross-linked by overnight incubation at 65 °C. The isolated DNA was RNase (NEB) treated and purified using QIAGEN columns. Libraries were generated using the NEBNext ChIP–seq Library Prep Master Mix Set for Illumina (NEB) and single-end sequencing reads (50 bp) were generated on HiSeq 2500 platforms (Illumina). ChIP–seq reads are available on NCBI GEO under accession number GSE72121. Raw reads were mapped to mouse reference genome GRCm38/mm10 using bowtie2 (version 2.2.3) and allowing a maximum of one mismatch[29]. Peaks for each sample were called using MACS2 algorithm (version 2.0.10.20131216)[30] using the shift size values calculated from the run_spp.R script from the SPP peak caller[31]. High quality peaks were identified using IDR2 (https://github.com/nboley/idr). A negative control ChIP was performed as described above using the Myt1l antibody on rtTA-only infected cells. Any rtTA peak that overlapped a peak in any other condition by greater than 50% was excluded from the final analyses. Heatmaps of ChIP–seq signals were generated around peak summits (±2 kb region) using 25-bp sliding windows with the HOMER suite (version 4.7)[32]. Read histograms, motif analysis, peak annotation, and gene ontology analysis were also performed using HOMER and PHANTER[33]. Both Bedtools and SAMtools were used for file processing and format conversions[34,35]. Differential Myt1l localization was determined using the DiffBind R package[36]. All ChIP–seq data were analysed from two or three biological replicates.

MNase–seq analysis. To assess nucleosome occupancy at candidate regions, we used a previously reported MEF MNase–seq data set (GSE40896)[25]. The raw reads were mapped to GRCm38/mm10 using bowtie (version 1.1.1) allowing one mismatch as described[37]. Histograms of read densities for the Myt1l peaks and Ascl1 peaks[8] (lifted over to mm10) were compiled using HOMER.

Transcript analysis using RNA-seq and quantitative PCR. RNA was isolated using Trizol (Invitrogen) and treated with DNase (NEB). For RNA-seq, libraries were prepared following the dUTP protocol[38] and paired-end sequencing reads (100 bp) were generated on HiSeq 2500 platforms (Illumina). RNA-seq reads are available on NCBI GEO under accession number GSE72121. Raw reads were mapped to mouse reference genome GRCm38/mm10 using TopHat2 (version 2.0.10)[39] and transcript assembly and differential expression determined using cufflinks (version 2.1.1) according to the cuffquant pipeline[40]. CummeRbund was used to generate expression scatterplots and cluster3 and treeview were used to generate heatmaps[41–43]. GSEA was performed using all genesets in the MsigDB database (GSE14012)[44,45], including a MEF gene signature that was compiled by taking the genes that were enriched by a factor of 10 in the MEF condition compared to the induced neuronal condition from the raw RNA-seq data in ref. 8 (Supplementary Table 3). The significance of GSEA profiles was determined by an FDR < 0.25, as described[45]. Cell-type-specific gene signatures were derived from the top 10% of the genes unique to a particular cell type[46–49], excluding any genes common amongst four out of five sets to exclude housekeeping genes (Supplementary Table 3). Odds ratio analysis was performed using the GeneOverlap R package (version 1.6.0)[50]. For quantitative PCR, RNA was reverse transcribed using Superscript II (Invitrogen) following the manufacturer's instructions. Quantitative real time PCR was performed from cDNA templates using the SYBR Green PCR master mix and a 7900HT Fast Real-Time PCR System (Applied Biosystems). Transcript levels were determined after normalization against GAPDH using the Relative Expression Software Tool (REST)[51]. A complete list of real-time PCR primers used in this study can be found in Supplementary Table 6. All RNA-seq data were analysed from two biological replicates.

SELEX. Constructs encoding Myt1l DNA-binding domains were generated by gene synthesis (codon optimized, Genscript) as indicated in Supplementary Table 5. Clones were transferred to an N-terminal thioredoxin hexahistidine bacterial expression vector (pETG-20A-SBP; ref. 52) by a Gateway LR reaction (Invitrogen). Proteins were produced in the *E. coli* Rosetta DE3 pLysS (Novagen), and purified, and HT-SELEX analyses were performed as described previously[53]. After each SELEX cycle, the selection ligands were sequenced using HiSeq 2000 platforms (Illumina), and PWM models generated using the seed, cycle and multinomial model reported in Supplementary Table 5 as described here[53].

Data availability statement. ChIP and RNA-seq data have been deposited in the NCBI GEO database under accession number GSE72121. All other data are available from the corresponding author upon reasonable request.

26. Maximov, A., Pang, Z. P., Tervo, D. G. R. & Südhof, T. C. Monitoring synaptic transmission in primary neuronal cultures using local extracellular stimulation. *J. Neurosci. Methods* **161,** 75–87 (2007).
27. Springer, M. L., Rando, T. A. & Blau, H. M. Gene delivery to muscle. *Curr. Protoc. Hum. Genet.* **13,** 13.4 (2002).

28. Dull, T. *et al.* A third-generation lentivirus vector with a conditional packaging system. *J. Virol.* **72,** 8463–8471 (1998).
29. Langmead, B. & Salzberg, S. L. Fast gapped-read alignment with Bowtie 2. *Nat. Methods* **9,** 357–359 (2012).
30. Zhang, Y. *et al.* Model-based analysis of ChIP-Seq (MACS). *Genome Biol.* **9,** R137 (2008).
31. Kharchenko, P. V., Tolstorukov, M. Y. & Park, P. J. Design and analysis of ChIP-seq experiments for DNA-binding proteins. *Nat. Biotechnol.* **26,** 1351–1359 (2008).
32. Heinz, S. *et al.* Simple combinations of lineage-determining transcription factors prime cis-regulatory elements required for macrophage and B cell identities. *Mol. Cell* **38,** 576–589 (2010).
33. Mi, H., Muruganujan, A., Casagrande, J. T. & Thomas, P. D. Large-scale gene function analysis with the PANTHER classification system. *Nat. Protocols* **8,** 1551–1566 (2013).
34. Li, H. *et al.* The Sequence Alignment/Map format and SAMtools. *Bioinformatics* **25,** 2078–2079 (2009).
35. Quinlan, A. R. & Hall, I. M. BEDTools: a flexible suite of utilities for comparing genomic features. *Bioinformatics* **26,** 841–842 (2010).
36. Ross-Innes, C. S. *et al.* Differential oestrogen receptor binding is associated with clinical outcome in breast cancer. *Nature* **481,** 389–393 (2012).
37. Langmead, B., Trapnell, C., Pop, M. & Salzberg, S. L. Ultrafast and memory-efficient alignment of short DNA sequences to the human genome. *Genome Biol.* **10,** R25 (2009).
38. Levin, J. Z. *et al.* Comprehensive comparative analysis of strand-specific RNA sequencing methods. *Nat. Methods* **7,** 709–715 (2010).
39. Kim, D. *et al.* TopHat2: accurate alignment of transcriptomes in the presence of insertions, deletions and gene fusions. *Genome Biol.* **14,** R36 (2013).
40. Trapnell, C. *et al.* Differential analysis of gene regulation at transcript resolution with RNA-seq. *Nat. Biotechnol.* **31,** 46–53 (2013).
41. de Hoon, M. J. L., Imoto, S., Nolan, J. & Miyano, S. Open source clustering software. *Bioinformatics* **20,** 1453–1454 (2004).
42. Goff, L. A., Trapnell, C. & Kelley, D. *CummeRbund: Visualization and Exploration of Cufflinks High-throughput Sequencing Data* (R package version 2.8.2., 2014).
43. Saldanha, A. J. Java Treeview–extensible visualization of microarray data. *Bioinformatics* **20,** 3246–3248 (2004).
44. Mootha, V. K. *et al.* PGC-1α-responsive genes involved in oxidative phosphorylation are coordinately downregulated in human diabetes. *Nat. Genet.* **34,** 267–273 (2003).
45. Subramanian, A. *et al.* Gene set enrichment analysis: a knowledge-based approach for interpreting genome-wide expression profiles. *Proc. Natl Acad. Sci. USA* **102,** 15545–15550 (2005).
46. Trapnell, C. *et al.* Transcript assembly and quantification by RNA-seq reveals unannotated transcripts and isoform switching during cell differentiation. *Nat. Biotechnol.* **28,** 511–515 (2010).
47. Bao, X. *et al.* A novel ATAC-seq approach reveals lineage-specific reinforcement of the open chromatin landscape via cooperation between BAF and p63. *Genome Biol.* **16,** 284 (2015).
48. Huang, L. *et al.* Partial hepatectomy induced long noncoding RNA inhibits hepatocyte proliferation during liver regeneration. *PLoS One* **10,** e0132798 (2015).
49. Zhang, Y. *et al.* An RNA-sequencing transcriptome and splicing database of glia, neurons, and vascular cells of the cerebral cortex. *J. Neurosci.* **34,** 11929–11947 (2014).
50. Shen, L. GeneOverlap: An R package to test and visualize gene overlaps (2014).
51. Pfaffl, M. W., Horgan, G. W. & Dempfle, L. Relative expression software tool (REST) for group-wise comparison and statistical analysis of relative expression results in real-time PCR. *Nucleic Acids Res.* **30,** e36 (2002).
52. Jolma, A. *et al.* DNA-binding specificities of human transcription factors. *Cell* **152,** 327–339 (2013).
53. Nitta, K. R. *et al.* Conservation of transcription factor binding specificities across 600 million years of bilateria evolution. *eLife* **4,** e04837 (2015).

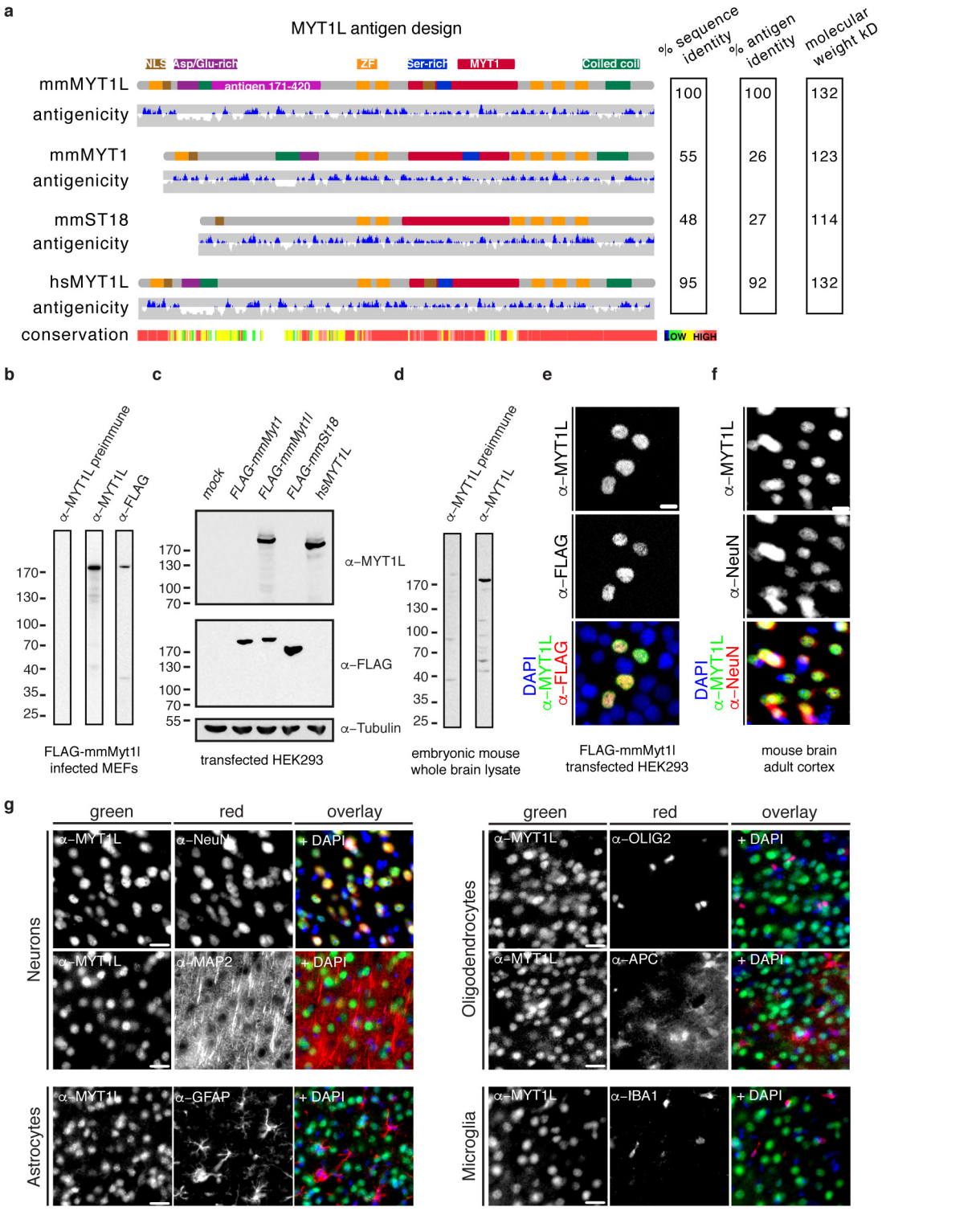

Extended Data Figure 1 | Myt1l antibody design and characterization. **a**, Schematic of mouse Myt1 family members mmMyt1 (Q8CFC2), mmMyt1l (P97500) and mmSt18 (A5LFV3) as well as human hsMyt1l homologue (Q9UL68). Highlighted are the nuclear localization signals (NLS), aspartic acid/glutamic acid-rich (Asp/Glu-rich), serine-rich (Ser-rich), Myt1 and coiled-coil domains and the CCHC-type zinc-fingers (ZF). Also shown is the predicted antigenicity and the conservation between the proteins generated using EpiC and T-Coffee, respectively. Based on these data, a fragment of mmMyt1l (amino acids 171–420) was used as an antigen for antibody induction in rabbits. The sequence identities among the antigen regions and the full-length proteins and their molecular masses are shown (right). **b**–**d**, Western blots of MEF cells upon induction of Flag-tagged mmMyt1l (**b**), HEK293 cells upon transfection of Flag-tagged mmMyt1, mmMyt1l, St18, and untagged hsMyt1l (**c**), and E13.5 embryonic mouse whole brain lysate using preimmune serum and antibodies against Myt1l, Flag, and tubulin (**d**). **e**, Microscopy images of HEK293 cells upon transfection of Flag-tagged mmMyt1l followed by immunofluorescence using antibodies against Flag (red) and Myt1l (green). **f**, Microscopy images of a section from adult mouse cortex upon immunofluorescence using antibodies against NeuN (red) and Myt1l (green), and DAPI staining (blue). Scale bar, 10 μm. **g**, Myt1l antibody specifically marks mouse brain neurons *in vivo*. Immunofluorescence microscopy images of adult mouse brain cortex sections using antibodies against neuron-specific NeuN and Map2 or oligodendrocyte-specific Olig2 and Apc. Astrocytes (Gfap) and microglia (Iba1) are shown in red with Myt1l (green) and DAPI staining (blue). Note that Myt1l overlaps only with neuronal markers. Scale bar, 20 μm.

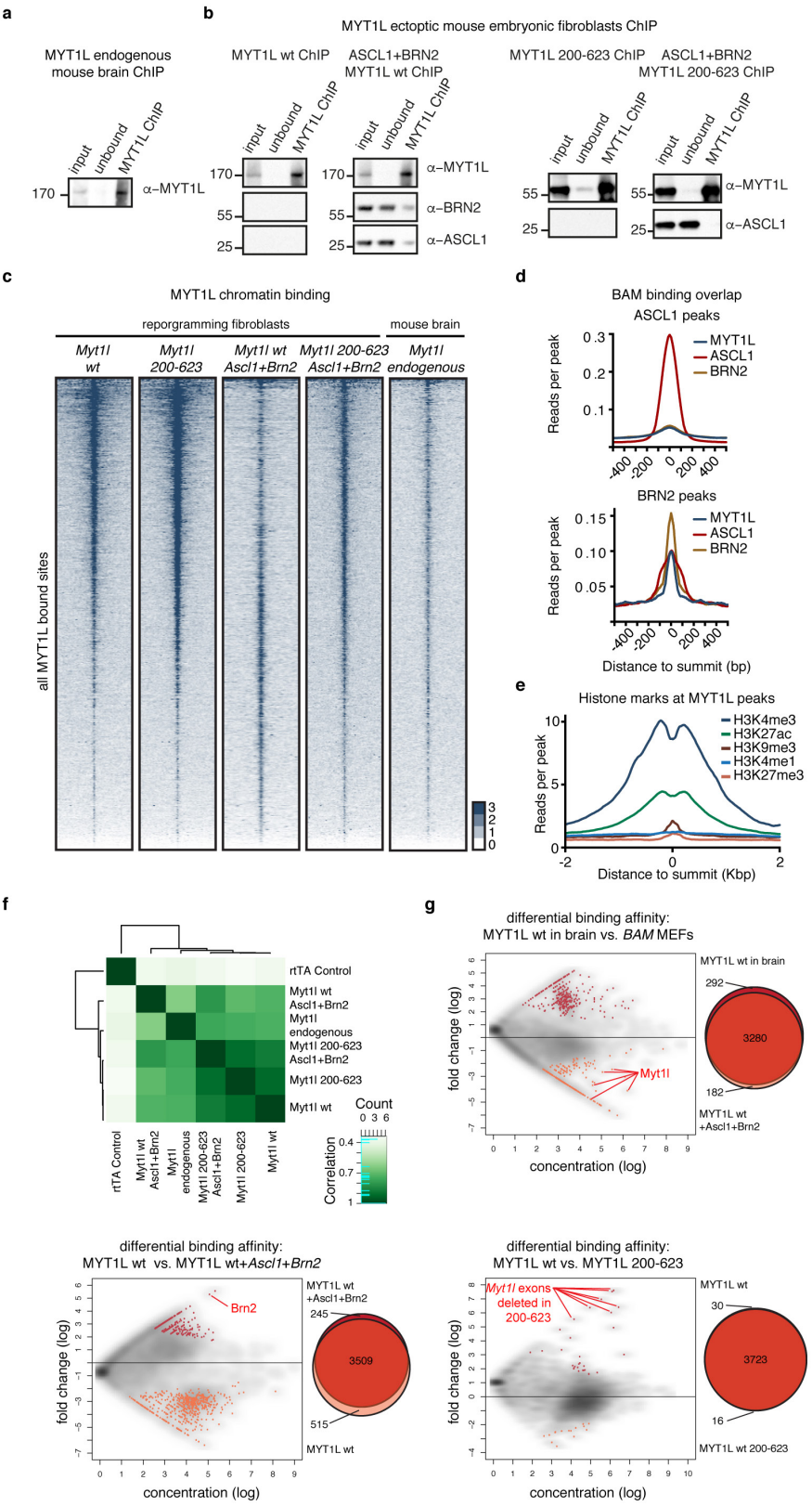

Extended Data Figure 2 | See next page for caption.

Extended Data Figure 2 | Genome-wide chromatin binding of Myt1l. **a**, **b**, ChIP of endogenous Myt1l from E13.5 mouse brain (**a**) or of wild-type Myt1l (**b**, left) and $Myt1l_{200–623}$ (**b**, right) transgenes from MEF cell lysates 2 days after induction with or without Ascl1 and Brn2. Chromatin immunoprecipitates were analysed by western blotting with Myt1l, Brn2, and Ascl1 antibodies. Input, 0.3% of ChIP input; unbound, 0.3% of ChIP flow-through; ChIP, 3% of ChIP eluates. **c**, ChIP–seq genome-wide occupancy of endogenous Myt1l in E13.5 mouse brains ($n = 2$) or Myt1l and $Myt1_{200–623}$ in MEFs two days after induction with ($n = 3$) or without ($n = 2$) Ascl1 and Brn2. A total of 6,911 peaks are sorted on the basis of intensity and corresponding genomic regions are displayed across all datasets; signal is displayed ± 2 kb from summits (see also Fig. 1). **d**, Chromatin reads for Myt1l, Ascl1 and Brn2 at Ascl1 (top) and Brn2 peaks (bottom)[8]. **e**, Chromatin reads of indicated histone marks in uninfected MEFs at the sites at which Myt1l is bound during reprogramming. Signal is displayed ± 2 kb from peak summit. **f**, Pearson correlation and clustering analysis of ChIP–seq samples highlight high binding overlap between different conditions. **g**, MA plots from DiffBind and corresponding Venn diagrams showing the distribution of Myt1l ChIP–seq peak intensities between indicated conditions; endogenous Myt1l in mouse brain versus overexpressed Myt1l in BAM MEFs (top), Myt1l overexpression alone versus in combination with Ascl1 and Brn2 (BAM) in MEFs (bottom left), and wild-type Myt1l versus $Myt1l_{200–623}$ overexpression in MEFs (bottom right). Significantly different peaks are shown in colour and numbers are annotated. Peaks that are significantly changed by the experimental setup are highlighted red.

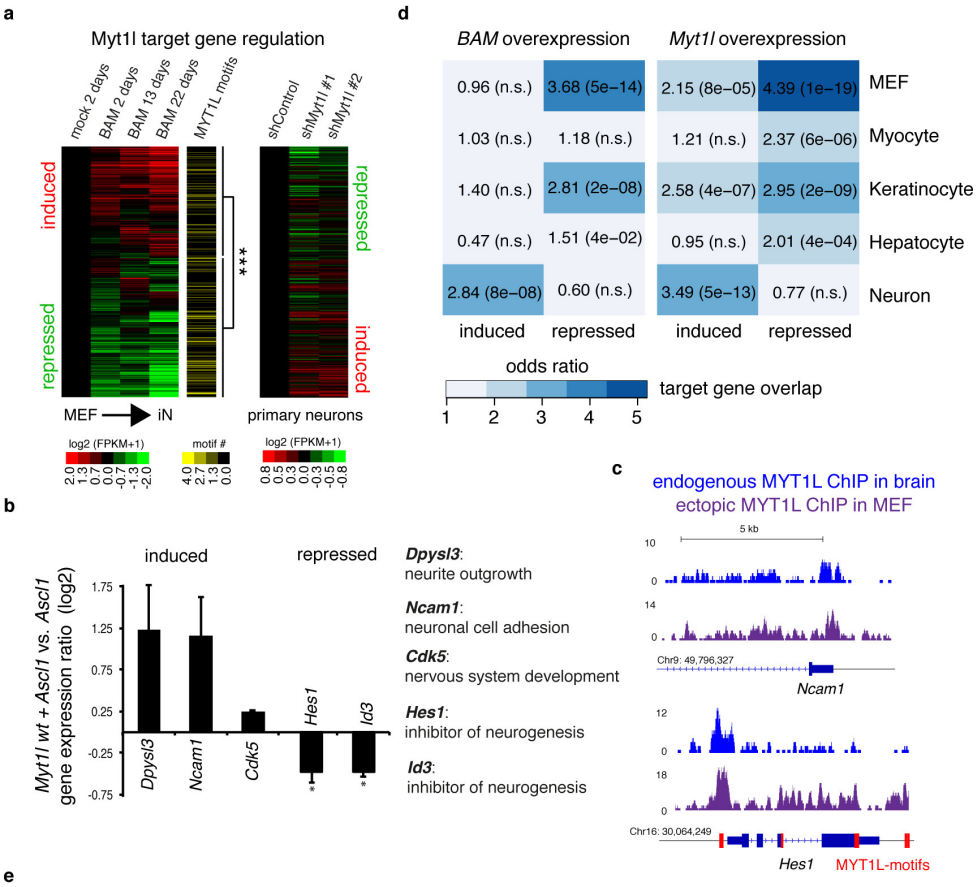

e

GO of MYT1L targets downregulated during iN formation	Enrichment	P-value
regulation of mesenchymal cell proliferation (GO:0010464)	6.09	2.43e-02
ribosome assembly (GO:0042255)	5.87	4.79e-03
regulation of cartilage development (GO:0061035)	5.69	2.59e-03
cardiac septum development (GO:0003279)	4.68	4.58e-04
response to transforming growth factor beta (GO:0071559)	4.02	1.70e-02
regulation of smooth muscle cell proliferation (GO:0048660)	3.60	3.98e-02
stem cell population maintenance (GO:0019827)	3.51	3.11e-02
heart morphogenesis (GO:0003007)	3.48	6.90e-06
regulation of nucleocytoplasmic transport (GO:0046822)	3.11	5.42e-03
peptide biosynthetic process (GO:0043043)	3.05	2.28e-07
lung development (GO:0030324)	3.03	2.17e-02
regulation of epithelial cell proliferation (GO:0050678)	3.01	5.97e-05
negative regulation of neuron differentiation (GO:0045665)	3.00	9.98e-03
respiratory tube development (GO:0030323)	2.98	2.80e-02
T cell activation (GO:0042110)	2.80	9.55e-03
embryonic organ morphogenesis (GO:0048562)	2.80	2.37e-04
cellular response to growth factor stimulus (GO:0071363)	2.80	1.60e-04
angiogenesis (GO:0001525)	2.75	2.68e-03
gland development (GO:0048732)	2.58	4.18e-04
circulatory system development (GO:0072359)	2.54	2.62e-11

GO of MYT1L targets upregulated during iN formation	Enrichment	P-value
histone modification (GO:0016570)	2.89	1.17e-02
chromosome organization (GO:0051276)	2.23	1.68e-04
RNA metabolic process (GO:0016070)	2.21	7.57e-21
protein transport (GO:0015031)	1.89	1.90e-02
positive regulation of nitrogen compound metabolic process (GO:0051173)	1.86	1.49e-05
organelle organization (GO:0006996)	1.73	1.58e-07
generation of neurons (GO:0048699)	1.73	3.15e-02
cellular macromolecule metabolic process (GO:0044260)	1.72	7.13e-20
cellular protein modification process (GO:0006464)	1.70	1.26e-04
regulation of cell communication (GO:0010646)	1.52	9.06e-03

Extended Data Figure 3 | See next page for caption.

Extended Data Figure 3 | Myt1l represses many genes but not the neuronal transcriptional network. a, Heatmap of gene expression changes at promoter-bound Myt1l target genes during iN cell conversion of MEFs at the indicated time points based on RNA-seq show significant enrichment of Myt1l motifs at repressed genes ($P = 6.85 \times 10^{-6}$), $n = 2$ (ref. 8) (left) and inverse transcriptional effects upon Myt1l knockdown in primary hippocampal neurons (right). **b**, Mean expression of selected Myt1l target genes in MEFs upon induction of wild-type Myt1l together with Ascl1 for two days determined by quantitative real-time PCR show significant repression of canonical inhibitors of neurogenesis by Myt1l. Names and annotated functions of tested genes are indicated, expression levels were normalized to Ascl1-only induction and GAPDH expression, $n = 4$ biological replicates (with 2 technical replicates each). Error bars show s.e.m., pair wise fixed reallocation randomization test $^{*}P < 0.001$ (ref. 51). **c**, Myt1l ChIP–seq profile at the *Hes1* and *Ncam1* promoter shows strong binding of endogenous Myt1l in E13.5 mouse brain and overexpressed wild-type Myt1l in MEFs two days after reprogramming; red bars mark multiple Myt1l AAGTTT motifs present in repressed *Hes1* promoter and gene body. **d**, Overlap of Myt1l-bound target genes that are induced or repressed during conversion of MEFs into iN cells upon overexpression of Myt1l with or without Ascl1 and Brn2 and indicated cell type-specific expression signatures determined by GeneOverlap[50]. Odds ratio >2 represents strong association, *P* values are shown in brackets; n.s., not significant. **e**, Selected top gene ontology (GO) terms of Myt1l-targeted genes that are repressed (top) or induced (bottom) during reprogramming determined by PANTHER[33]. Enrichment scores and *P* values are shown. Highlighted are the terms 'negative regulation of neuron differentiation' (green) in the repressed cluster and 'generation of neurons' (red) in the induced cluster. Both analyses show a striking enrichment of repressed Myt1l target genes within several non-neuronal programs. Of note, several metabolic GO terms are among the upregulated target genes.

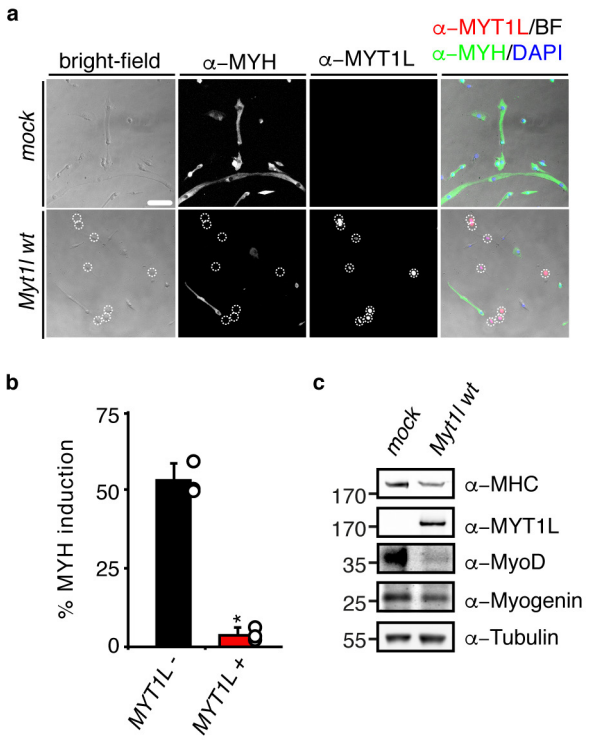

Extended Data Figure 4 | Myt1l blocks muscle differentiation in primary myoblasts. a, Representative micrographs of muscle cells derived from primary myoblasts upon differentiation for 4 days with with rtTA alone (mock) or in combination with wild-type Myt1l followed by immunofluorescence using antibodies against Myh (green), Myt1l (red) and DAPI staining (blue); scale bar, 100 μm. **b**, Muscle differentiation efficiency of cells shown in **a** highlight the repressive effect of Myt1l expression (+) on Myh-induction compared to Myt1l-negative cells (−). $n = 3$, error bars show s.e.m., t-test $^*P < 0.005$. **c**, Western blot of muscle cells shown in **a** using indicated antibodies shows reduction of several muscle markers upon Myt1l overexpression.

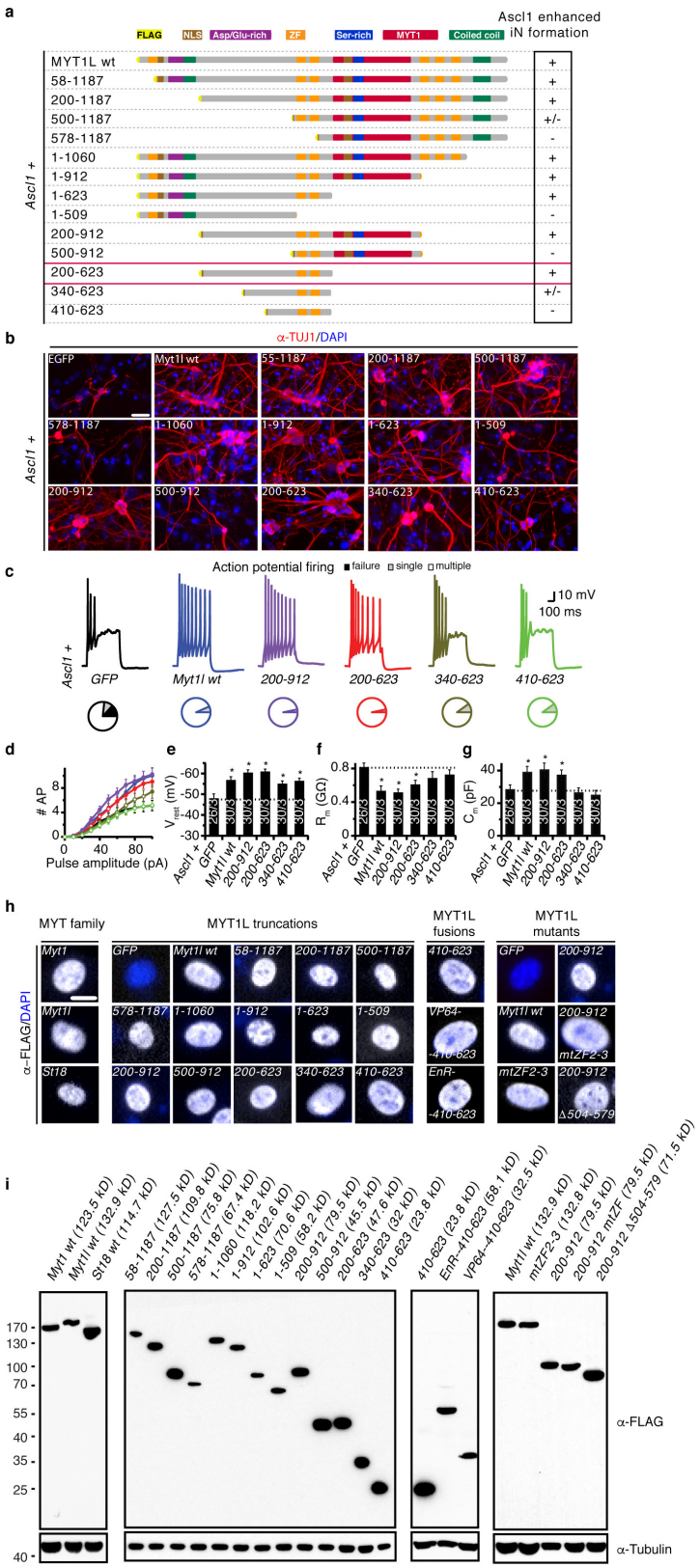

Extended Data Figure 5 | See next page for caption.

Extended Data Figure 5 | Truncation screen identifies minimal neurogenic domains of Myt1l. a, Schematic of Flag- and NLS-tagged Myt1l truncation proteins including amino acid positions. Ability to enhance neurogenic conversion together with Ascl1 is indicated by (+), minimal active truncation Myt1l$_{200–623}$ is boxed red (see also Fig. 3). Myt1l truncations with partial or without enhanced conversion activity are indicated with (+/−) and (–), respectively. **b**, Representative micrographs of iN cells derived from MEFs upon reprogramming for 14 days with Ascl1 together with the indicated transgenes followed by immunofluorescence using antibodies against TUJ1 (red) and DAPI staining (blue); scale bar, 50 μm. **c**–**g**, Electrophysiological characterization of iN cells derived in **b** upon maturation for 21 days on mouse glia. **c**, Representative action potential (AP) traces of iN cells upon reprogramming with Ascl1 together with indicated Myt1l truncation. Pie charts indicate fraction of cells firing single (grey), multiple (white), or no (black) action potentials. **d**, Mean number of action potentials fired plotted with respect to pulse amplitude measured at −60 mV holding potential. **e**, Mean resting membrane-potential (V_{rest}). **f**, **g**, Mean membrane resistance (R_m; **f**) and capacitance (C_m; **g**) measured at −70 mV holding potential. Dotted line indicates intrinsic properties of Ascl1 + GFP cells; $n = 3$ biological replicates (total number of individual cells measured indicated), error bars show s.e.m., t-test $^*P < 0.05$. **h**, Microscopy images showing nuclear localization of all tested Myt1l truncations 2 days after induction in MEFs by immunofluorescence using antibodies against Flag (grey) and DAPI staining (blue), scale bar 10 μm. **i**, Western blot analysis of HEK293 cells 2 days after transfection with the indicated transgenes confirms protein integrity using antibodies against Flag and tubulin.

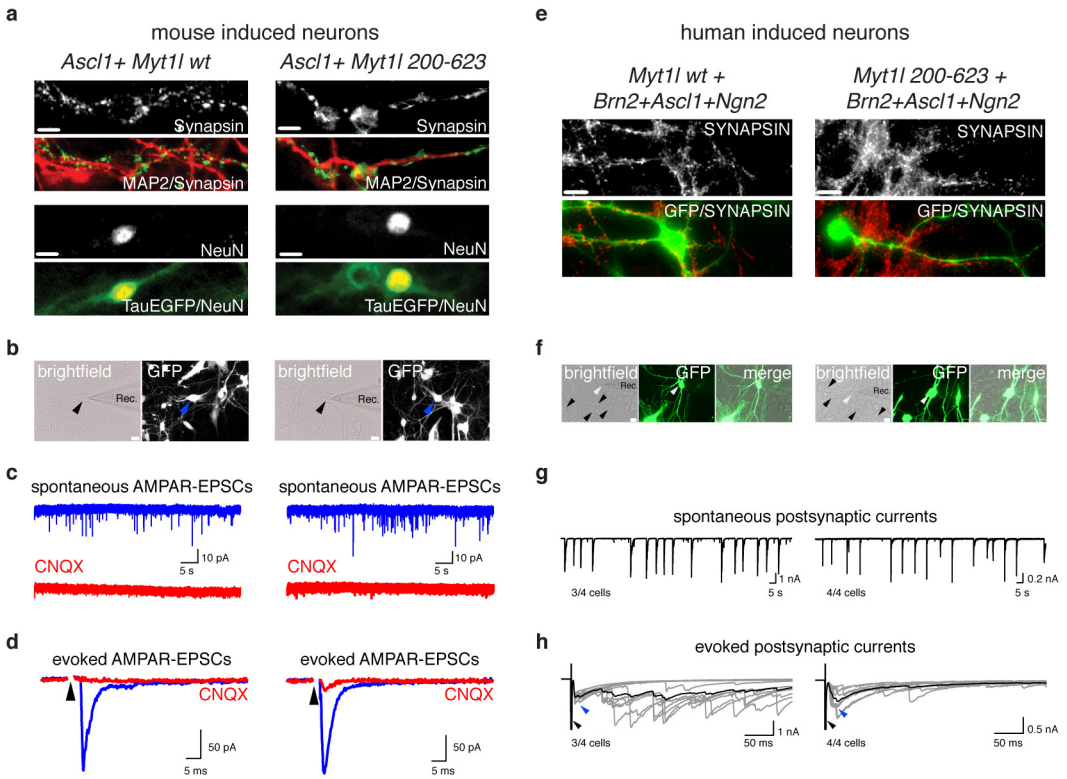

Extended Data Figure 6 | Characterization of mouse and human iN cells generated with Ascl1 and Myt1l. a, Microscopy images of iN cells derived from MEFs upon reprogramming for 21 days on mouse glia by overexpression of Ascl1 together with either wild-type Myt1l or $Myt1l_{200–623}$ followed by immunofluorescence using antibodies against Map2 (red) and synapsin (green) or NeuN (red) and Tau–eGFP (green), scale bar 10 μm. **b**, Synaptic recordings of Tau–eGFP-positive mouse iN cells shown in **a**. **c**, **d**, Spontaneous and evoked EPSCs were recorded at a holding potential of −70 mV (blue) and blocked by the addition of CNQX (red), indicating that the excitatory nature of the resulting induced neurons is mediated through AMPA-type receptors (AMPARs). **e**, Immunofluorescence images of iN cells derived from human embryonic fibroblasts upon reprogramming for 6 weeks by overexpression of GFP, Ascl1, Ngn2 and Brn2 together with either wild-type Myt1l or $Myt1l_{200–623}$ and co-culture with primary cortical mouse neurons using antibodies against synapsin (red) and GFP (green); scale bar,10 μm. **f**, Synaptic recordings of GFP-positive human iN cells shown in **e**. **g**, **h**, Spontaneous and evoked EPSCs were recorded at a holding potential of −70 mV, indicating synaptic competence of the resulting induced human neurons. $n = 4$ cells (fraction of active cells indicated).

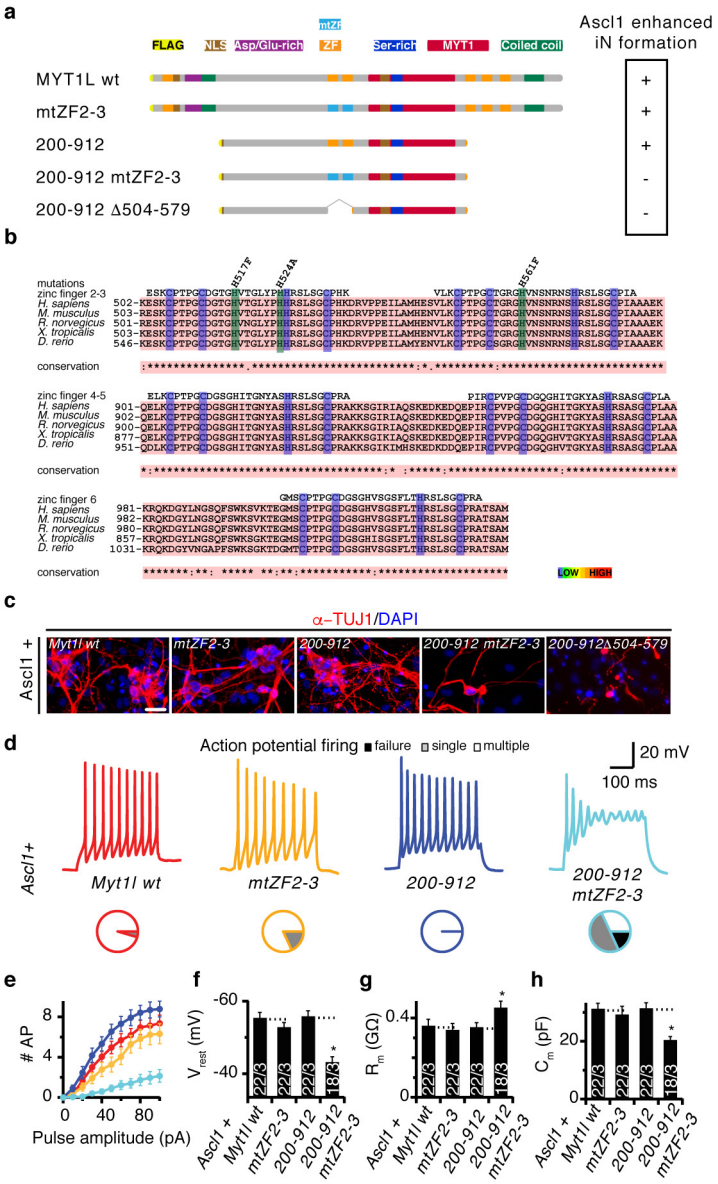

Extended Data Figure 7 | Zinc-fingers are essential for neurogenic function of Myt1l. a, Schematic of Myt1l zinc-finger 2–3 point and deletion mutants. The ability to enhance neurogenic conversion together with Ascl1 is indicated by (+), non-functional mutants are indicated with (−) (see also Fig. 3). **b**, Sequence alignments and conservation of CCHC-type zinc-fingers from Myt1l; cysteine and histidine residues that can coordinate Zn(II) are highlighted in purple, non-coordinating mutated histidines are shown in green. **c**, Representative immunofluorescence of iN cells derived from MEFs upon reprogramming for 14 days with Ascl1 and the indicated transgenes; TUJ1 (red), DAPI staining (blue), scale bar, 50 μm. **d**–**h**, Electrophysiological characterization of iN cells derived in **c** upon maturation for 21 days on mouse glia. **d**, Representative action potential (AP) traces of iN cells generated with indicated transgenes; pie charts indicate fraction of cells firing single (grey), multiple (white), or no (black) action potentials. **e**, Mean number of action potentials fired plotted with respect to pulse amplitude measured at −60 mV holding potential. **f**, Mean resting membrane potential (V_{rest}). **g**, **h**, Mean membrane resistance (R_m; **g**) and capacitance (C_m; **h**) measured at −70 mV holding potential. Dotted line indicates intrinsic properties of Ascl1 + wild-type Myt1l or Ascl1 + Myt1l$_{200–912}$ cells; $n = 3$ biological replicates (total number of individual cells measured indicated), error bars show s.e.m., t-test $^*P < 0.05$.

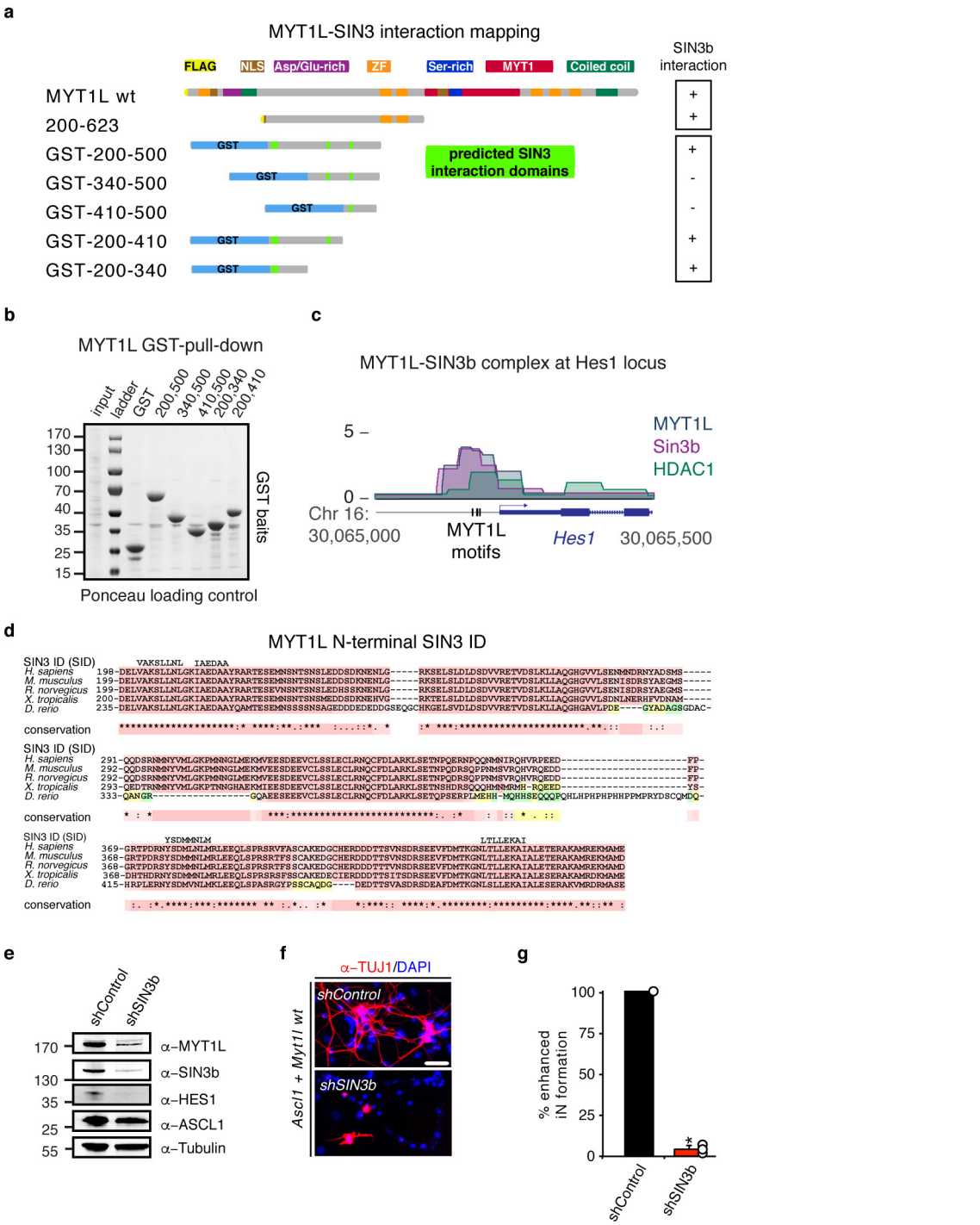

Extended Data Figure 8 | Sin3b binds Myt1l via N-terminal SID domains and is essential for reprogramming. a, Schematic of FLAG and NLS-tagged Myt1l truncations and GST-tagged Myt1l fusion proteins. Putative SIN3 interaction domains (SIDs) are highlighted (see also Fig. 3). Ability and inability to interact biochemically with Sin3b are indicated by (+) and (−), respectively. **b**, GST bait loading after pull down was controlled by Ponceau staining of the western blot membrane. Input, 0.2% of pull down input; pull down lanes, 20% of pull down eluates. **c**, ChIP–seq tracks of Sin3b, HDAC1, and Myt1l show binding at the *Hes1* promoter 2 days after MEF reprogramming with Ascl1, Brn2 and wild-type Myt1l. Vertical bars mark Myt1l AAGTT motifs. **d**, Multiple sequence alignments of the highly conserved putative SIDs within minimal functional region of Myt1l from selected eukaryotic species. The alignment was generated using T-Coffee and putative SID regions are shown above the alignment. **e**, Western blot of iN cells derived from MEFs upon reprogramming for 2 days with Ascl1 and wild-type Myt1l together with either control or *Sin3b*-targeting shRNA constructs using indicated antibodies. **f**, Representative micrographs of iN cells derived in **e** upon reprogramming for 14 days followed by immunofluorescence using antibodies against TUJ1 (red) and DAPI staining (blue); scale bar, 50 μm. **g**, Conversion efficiency of cells shown in **f** based on TUJ1-positive cells with neuronal morphology highlight the deleterious effect of *Sin3b* knockdown on iN cell formation. $n = 3$, error bars show s.e.m., *t*-test $^*P < 0.005$.

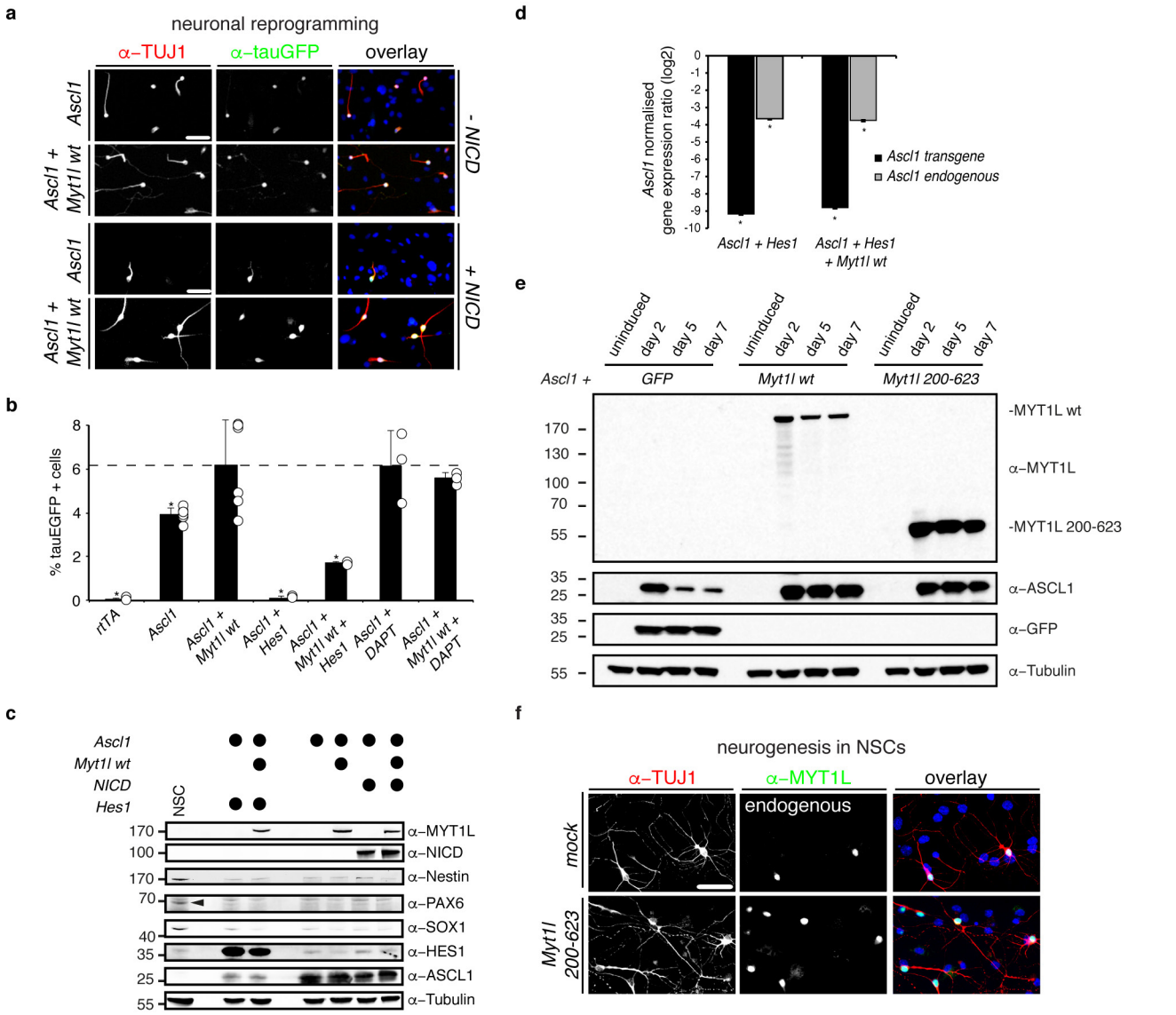

Extended Data Figure 9 | Myt1l acts upstream of Hes1 to repress Notch signalling and stabilize Ascl1. a, Immunofluorescence of iN cells quantified in Fig. 4a derived from MEFs upon reprogramming for 7 days with Ascl1 and wild-type Myt1l, NICD or a combination; TUJ1 (red), Tau–eGFP (green), DAPI staining (blue); scale bar, 50 μm. **b**, Neurogenic conversion efficiency of MEF cells upon reprogramming for 7 days with Ascl1 together with either wild-type Myt1l ($n = 6$), Hes1 ($n = 3$) or a combination of indicated transgenes or upon treatment with DAPT (10 μM) ($n = 3$) based on Tau–eGFP induction determined by flow cytometry. Dotted line indicates mean conversion efficiency of Ascl1 + Myt1l cells; error bars show s.d., *t*-test $^*P < 0.05$. **c**, Western blot analysis of cells shown in **a** and **b** after 2 days of reprogramming and mouse NSCs using indicated antibodies shows no striking induction of the neural stem-cell markers nestin, Pax6 (arrowhead) or Sox1 in any condition but strong reduction of Ascl1 upon *Hes1* overexpression. **d**, Mean expression levels of endogenous and exogenous (overexpressed) *Ascl1* transcripts in MEFs upon overexpression of *Ascl1* and *Hes1* with or without wild-type *Myt1l* for 2 days determined by quantitative real time PCR show significant repression of both endogenous and exogenous *Ascl1* by *Hes1* overexpression independent of *Myt1l*. Expression levels were normalized to *Ascl1* only induction and GAPDH expression. $n = 4$ biological replicates (with 4 technical replicates each), error bars show s.e.m., pair-wise fixed reallocation randomization test $^*P < 0.001$ (ref. 51). **e**, Western blot analysis of MEF cells upon induction of Ascl1 together with GFP, wild-type Myt1l or $Myt1l_{200–623}$ after 0, 2, 5 and 7 days of reprogramming using antibodies against Myt1l, Ascl1, GFP and tubulin shows no striking induction of full-length Myt1l upon overexpression of minimal fragment but stabilization of Ascl1 levels. **f**, Immunofluorescence of neurons quantified in Fig. 4c derived from mouse NSCs upon differentiation for 7 days with rtTA alone (mock) or in combination with $Myt1l_{200–623}$; TUJ1 (red), Myt1l (green), DAPI staining (blue), scale bar 50 μm. Of note, all neurons formed in the control condition expressed endogenous Myt1l.

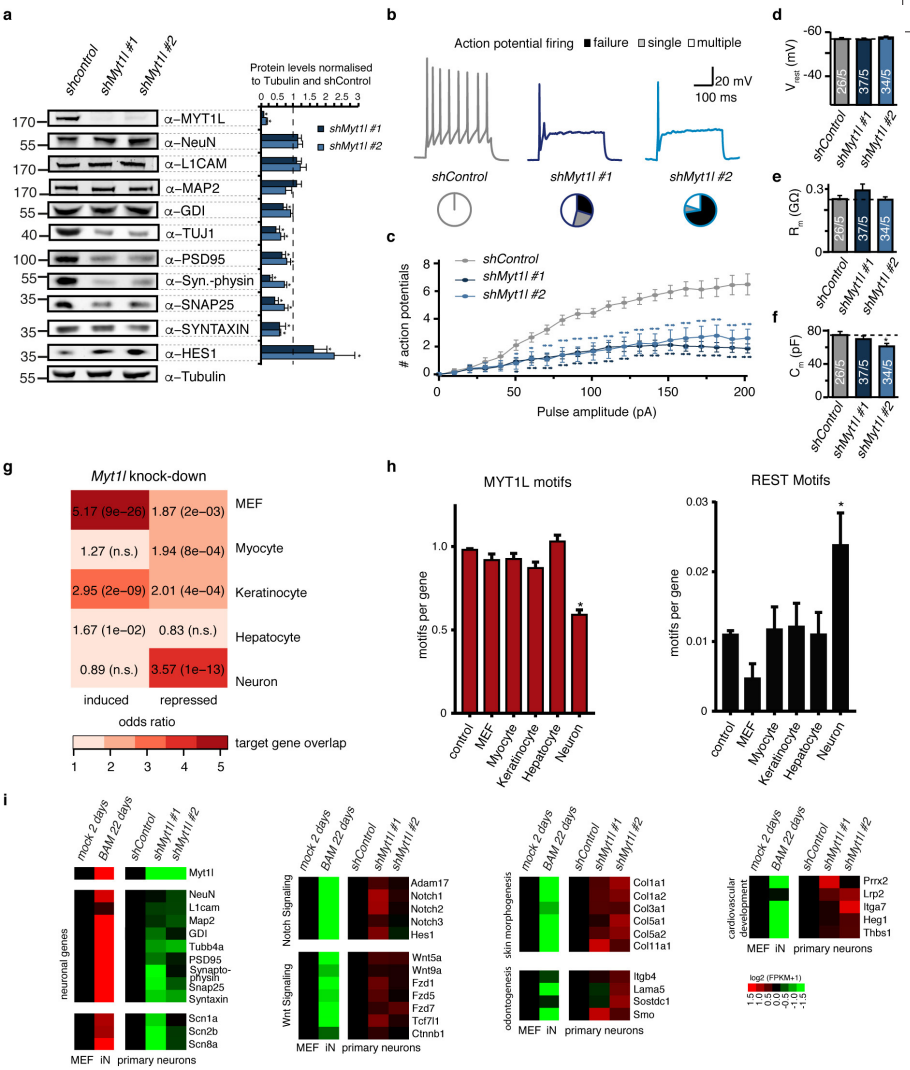

j

GO of Myt1l targets downregulated upon Myt1l knock-down in primary neurons	Enrichment	P-value
regulation of DNA-templated transcription in response to stress (GO:0043620)	9.68	6.24E-05
organelle fusion (GO:0048284)	4.99	8.73E-04
response to oxygen levels (GO:0070482)	3.59	3.83E-02
transmembrane receptor protein serine/threonine kinase signaling pathway (GO:0007178)	3.57	4.13E-02
learning or memory (GO:0007611)	3.36	5.93E-03
positive regulation of apoptotic process (GO:0043065)	2.61	5.31E-04
positive regulation of RNA metabolic process (GO:0051254)	2.04	2.82E-05
protein transport (GO:0015031)	2.00	4.20E-03
positive regulation of macromolecule biosynthetic process (GO:0010557)	1.95	4.94E-05
positive regulation of nitrogen compound metabolic process (GO:0051173)	1.93	1.93E-05
cellular protein modification process (GO:0006464)	1.83	5.11E-06
protein modification process (GO:0036211)	1.83	5.11E-06
generation of neurons (GO:0048699)	1.80	1.31E-02

GO of Myt1l targets upregulated upon Myt1l knock-down in primary neurons	Enrichment	P-value
regulation of cartilage development (GO:0061035)	6.18	3.38E-04
negative regulation of protein binding (GO:0032091)	4.69	1.04E-02
nucleosome organization (GO:0034728)	4.21	1.87E-02
stem cell population maintenance (GO:0019827)	3.72	7.21E-03
ribosome biogenesis (GO:0042254)	3.39	1.31E-05
heart morphogenesis (GO:0003007)	2.94	9.06E-03
regulation of epithelial cell proliferation (GO:0050678)	2.87	4.26E-04
negative regulation of neurogenesis (GO:0050768)	2.79	4.61E-03
embryonic organ morphogenesis (GO:0048562)	2.71	3.70E-03
RNA processing (GO:0006396)	2.66	9.85E-10
heart development (GO:0007507)	2.31	1.58E-03
tube development (GO:0035295)	2.08	1.35E-02
circulatory system development (GO:0072359)	2.03	5.63E-04

Extended Data Figure 10 | See next page for caption.

Extended Data Figure 10 | Myt1l maintains neuronal identity by repression of non-neuronal programs. a, Myt1l knockdown in P0 mouse primary hippocampal neuronal cultures impairs neuronal maturation and maintenance. Cells were infected with shRNA-expressing lentivirus on third day of *in vitro* culture and analysed 11 days later by quantitative western blot using indicated antibodies. While tubulin served as loading control, several neuronal markers were severely downregulated by Myt1l depletion. Representative western blot images are shown, $n = 5$, error bars show s.e.m., *t*-test $^*P < 0.05$. **b**–**f**, Electrophysiological characterization of Myt1l knockdown neurons derived in **a**. **b**, Representative action potential (AP) traces of hippocampal neurons upon indicated knockdown; pie charts indicate fraction of cells firing single (grey), multiple (white), or no (black) action potentials at the 90 pA pulse. **c**, Mean number of action potentials fired, plotted with respect to pulse amplitude measured at −60 mV holding potential. **d**, Mean resting membrane-potential (V_{rest}). **e**, **f**, Mean membrane resistance (R_m; **e**) and capacitance (C_m; **f**) measured at −70 mV holding potential. Dotted line indicates intrinsic properties upon control shRNA treatment. $n = 5$ biological replicates (total number of individual cells measured indicated), error bars show s.e.m., *t*-test $^*P < 0.05$. **g**, Myt1l knockdown in P0 mouse primary hippocampal neuronal cultures induces non-neuronal gene expression programs. Overlap of Myt1l-bound target genes that are induced or repressed upon knock down of Myt1l in primary hippocampal neurons and indicated cell type-specific expression signatures determined by GeneOverlap[50]. Odds ratio >2 represents strong association, *P* values are shown; n.s., not significant. **h**, Relative number of Myt1l and REST DNA binding motifs at cell type specific-genes highlight depletion of Myt1l and enrichment of REST motifs at neuronal genes (*t*-test $^*P < 0.005$). **i**, RNA–seq analysis of genes shown in **a**, confirm decreased expression of neuronal genes upon Myt1l depletion. In addition several Notch and Wnt signalling factors that are direct targets of Myt1l are de-repressed (see also Fig. 2c). In addition, transcription of several non-neuronal lineage specifiers is induced compared to the control. Shown are gene expression values of cells treated as in **a** based on RNA–seq; fold change is represented in logarithmic scale normalized to the control shRNA-treated sample, $n = 2$. **j**, Selected top gene ontology (GO) terms of Myt1l-targeted genes that are repressed (top) or induced (bottom) upon knock down in primary hippocampal neurons determined by PANTHER[33]. Enrichment scores and *P* values are shown. Highlighted are the terms 'generation of neurons' (green) in the repressed cluster and 'negative regulation of neurogenesis' (red) in the induced cluster. In addition this analysis highlights induction of several non-neuronal gene expression programs upon Myt1l depletion.